Three-quarter Dirac points, Landau levels, and magnetization in α-(BEDT-TTF)₂I₃

Keita Kishigi[*]

Faculty of Education, Kumamoto University, Kurokami 2-40-1, Kumamoto 860-8555, Japan

Yasumasa Hasegawa

Department of Material Science, Graduate School of Material Science, University of Hyogo, Hyogo 678-1297, Japan

The energies as a function of the magnetic field (H) and the pressure are studied theoretically in the tight-binding model for the two-dimensional organic conductor α-(BEDT-TTF)₂I₃, in which massless Dirac fermions are realized. The effects of the uniaxial pressure (P) are studied by using the pressure-dependent hopping parameters. The system is semimetallic with the same area of an electron pocket and a hole pocket at $P < 3.0$ kbar, where the energies (ε_D^0) at the Dirac points locate below the Fermi energy (ε_F^0) when $H = 0$. We find that at $P = 2.3$ kbar the Dirac cones are critically tilted. In that case a type of band crossing occurs at "three-quarter" Dirac points; i.e., the dispersion is quadratic in one direction and linear in the other three directions. We obtain magnetic field dependencies of the Landau levels (ε_n): $\varepsilon_n - \varepsilon_D^0 \propto (nH)^{4/5}$ at $P = 2.3$ kbar (three-quarter Dirac points) and $|\varepsilon_n - \varepsilon_F^0| \propto (nH)^2$ at $P = 3.0$ kbar (the critical pressure for the semimetallic state). We also study the magnetization as a function of the inverse magnetic field. We obtain two types of quantum oscillations. One is the usual de Haas–van Alphen (dHvA) oscillation, and the other is the unusual dHvA-like oscillation which is seen even in the system without the Fermi surface.

I. INTRODUCTION

α-(BEDT-TTF)₂I₃ is a two-dimensional organic conductor [1,2] that has attracted interest recently due to the realization of massless Dirac fermions [3–8]. There are four BEDT-TTF molecules in the unit cell, as shown in Fig. 1, and four energy bands are constructed by the highest occupied molecular orbits (HOMOs) of BEDT-TTF molecules. The electron bands are 3/4 filled, since one electron is removed from two BEDT-TTF molecules. Therefore, the system is semimetallic when the third and the fourth bands overlap, and it is an insulator when there is a gap between two bands.

Katayama, Kobayashi, and Suzumura [3] have theoretically shown the realization of massless Dirac fermions in α-(BEDT-TTF)₂I₃, where the third and the fourth bands touch at two Dirac points. Two bands near the Fermi energy can be approximately described by the tilted Weyl equation [4]. The existence of massless Dirac fermions in α-(BEDT-TTF)₂I₃ has been confirmed experimentally [5–8].

The energy dispersion of massless Dirac fermions near the Dirac points is linear, which is called a Dirac cone. Recently, by considering the anisotropy of the nearest-neighbor hoppings on a honeycomb lattice [9,10] it has been found that the dispersion is quadratic in two directions and linear in the two other directions when two Dirac points merge at a time-reversal-invariant point. That special point was named the semi-Dirac point in VO₂/TiO₂ nanostructures [11]. The semi-Dirac point has been also shown to exist in α-(BEDT-TTF)₂I₃ at high pressure theoretically [12,13].

When the magnetic field (H) is applied to two-dimensional systems, the energies are quantized. In many papers the effects of the magnetic field have been studied semiclassically [14] which is explained in Appendix A. However, a treatment in a quantum mechanical manner is possible for simple cases. For

example, the energies are given by

$$\varepsilon_n^{(\text{massive})} \propto \left(n + \tfrac{1}{2}\right)H, \quad n = 0,1,2 \tag{1}$$

for two-dimensional massive free electrons [15] and

$$\varepsilon_n^{(\text{Dirac})} \propto \text{sgn}(n)\sqrt{|n|H}, \quad n = 0, \pm 1, \pm 2, \dots \tag{2}$$

for massless Dirac fermions [graphene [16,17] and α-(BEDT-TTF)₂I₃ [18,19], where the linearization of the energy dispersion has been done]. Moreover, on the honeycomb lattice with the semi-Dirac point, Dietl, Piechon, and Montambaux [10] have found magnetic field dependencies that are given by

$$\varepsilon_n^{(\text{semi-Dirac})} \propto \text{sgn}(n)g(n)\left(\left|n + \frac{1}{2}\right|H\right)^{\frac{2}{3}},$$
$$n = 0, \pm 1, \pm 2, \dots, \tag{3}$$

where $g(0) \simeq 0.808$, $g(\pm 1) \simeq 0.994$, and $g(n) \simeq 1$ for $|n| \geqslant 2$.

In this study, we show the existence of a type of band crossing that we denote "three-quarter" Dirac points because the dispersion relation is quadratic in one direction and linear in the other three directions. Furthermore, we study the magnetic field dependencies of the energy in various cases of semimetallic state, critically tilted Dirac cones, massless Dirac fermions, and massive Dirac fermions.

In the tight-binding electrons, rich structures such as the broadening of the Landau levels (Harper broadening [20]) and recursive gap structures are seen on the square lattice [21–23] and on the honeycomb lattice [24–26]. These characteristic graphs are called the Hofstadter butterfly diagrams. Recently, we have studied the de Haas–van Alphen (dHvA) oscillation [15] in the tight-binding model for (TMTSF)₂NO₃ where electron and hole pockets coexist [27–29]. In that system the dHvA oscillation has been usually studied in the phenomenological theory of magnetic breakdown [30,31] and the Lifshitz and Kosevich (LK) formula [32,33]. The dHvA oscillation and the
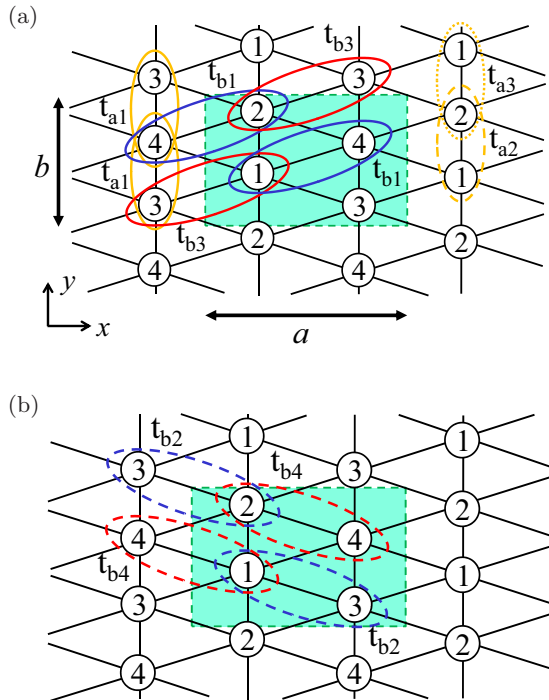
---

*Corresponding author: kishigi@educ.kumamoto-u.ac.jp

FIG. 1. The schematic figure of the tight-binding model for α-(BEDT-TTF)$_2$I$_3$. The unit cell is the rectangle in (a) and (b). The transfer integrals (t_{a1}, t_{a2}, t_{a3}, t_{b1}, t_{b2}, t_{b3}, and t_{b4}) are shown as ovals.

LK formula [34–37] are explained in Appendix B. We have shown that the magnetic field dependence of the amplitude of the dHvA oscillation at zero temperature is different from that of the LK formula due to the Harper broadening [38]. We have also obtained the dHvA-like oscillation on the honeycomb lattice even if the system is an insulator [26]. We investigate the oscillation of the magnetization in the Hofstadter butterfly diagrams for α-(BEDT-TTF)$_2$I$_3$ in this paper.

In α-(BEDT-TTF)$_2$I$_3$, the metal-insulator transition is observed at $T = 135$ K, which is thought to be caused by the charge ordering [39–42]. The metal-insulator transition is suppressed by pressure. Tajima *et al.* have observed from the conductivity that the charge ordering disappears at a uniaxial pressure, $P \gtrsim 10$ kbar [43]. In the hydrostatic pressure, the charge ordering has not been observed above 17 kbar from the magnetoconductivity [44] and above 11–12 kbar from the optical investigations [45] and conductivity [46]. In this paper we do not study the interaction between electrons, so we are not concerned with the metal-insulator transition caused by the charge ordering.

II. ENERGY BAND AND UNIAXIAL PRESSURE EFFECT

The energies of α-(BEDT-TTF)$_2$I$_3$ are described by the two-dimensional tight-binding model. The transfer integrals are taken between neighboring sites as shown in Fig. 1 and they are given as functions of pressure as the interpolation formulas [3,13,47–50]. In this study, we use the following interpolation formula [13,47,48] (hereafter, we employ eV and kbar as the units of transfer integrals and the pressure, respectively):

$$t_{a1} = -0.028(1.0 + 0.089P),$$
$$t_{a2} = -0.048(1.0 + 0.167P),$$

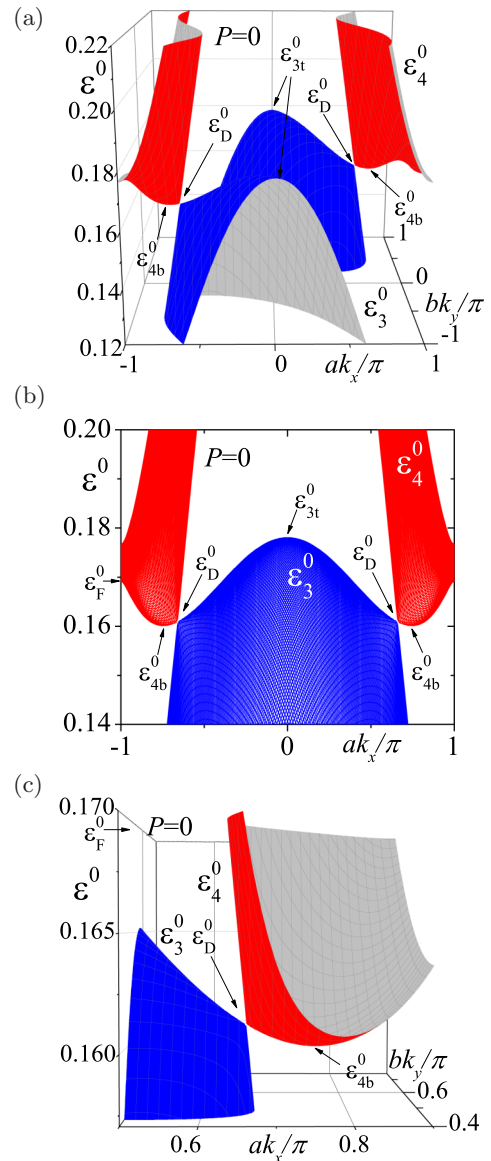FIG. 2. (a) The third and fourth energy bands (ε_3^0 and ε_4^0) at $P = 0$, where $\varepsilon_{3t}^0 \simeq 0.17805$, $\varepsilon_D^0 \simeq 0.16094$, and $\varepsilon_{4b}^0 \simeq 0.16011$. (b) is a view of (a) from a distant viewpoint along the k_y axis. (c) is an enlarged view of (a) near the Dirac point, $\mathbf{k}_D$.

$$t_{a3} = 0.020(1.0 - 0.025P),$$
$$t_{b1} = 0.123,$$
$$t_{b2} = 0.140(1.0 + 0.011P),$$
$$t_{b3} = 0.062(1.0 + 0.032P),$$
$$t_{b4} = 0.025, \tag{4}$$

where P is the uniaxial strain along the y axis. The Hamiltonian in this tight-binding model is explained in Appendix C for $h = 0$ and in Appendix D for $h \neq 0$.

By using the pressure-dependent hoppings [Eq. (4)] we show the third band and the fourth band at $P = 0, 3.0, 5.0, 39.2$, and 50 in Figs. 2–6. These contour plots except for the case of $P = 50$ are shown in Figs. 7–10. Katayama, Kobayashi, and Suzumura [3] have shown that at $P \geqslant 3.0$ the third band and
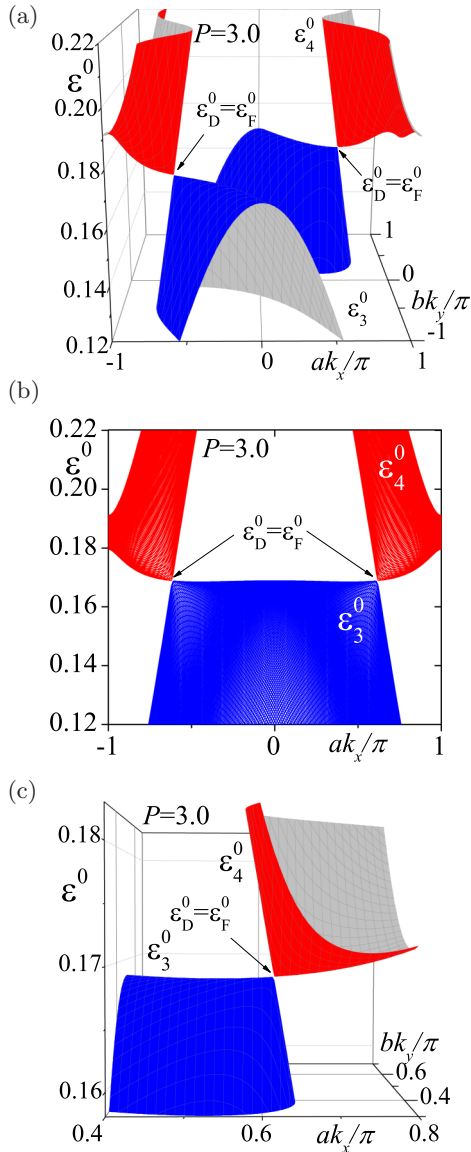
FIG. 3. The same as Fig. 2 except for $P = 3.0$, where $\varepsilon_{3t}^0 = \varepsilon_{4b}^0 = \varepsilon_D^0 = \varepsilon_F^0 \simeq 0.16887$.
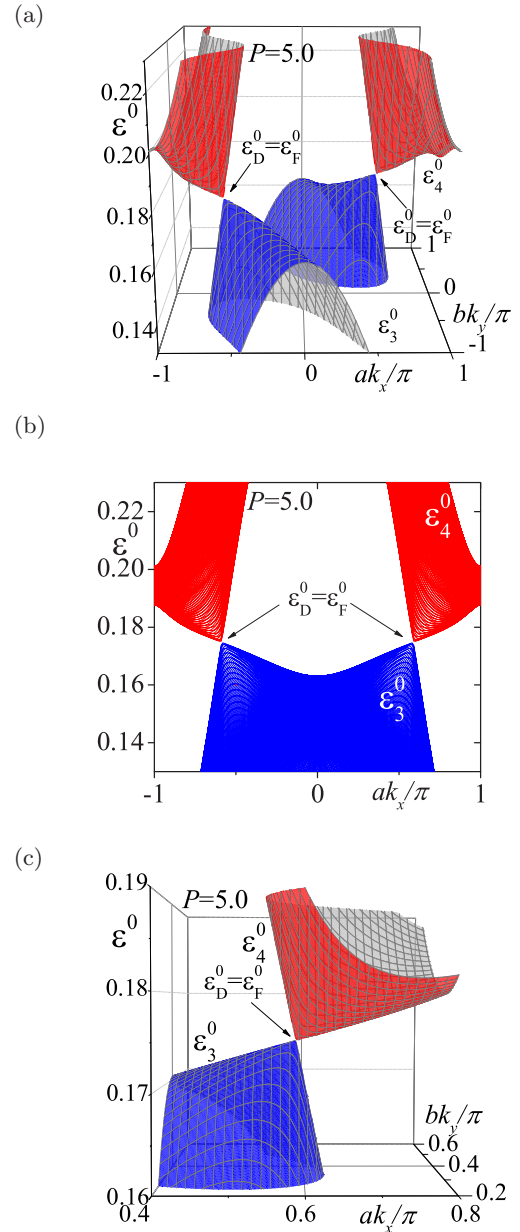

FIG. 4. The same as Fig. 2 except for $P = 5.0$, where $\varepsilon_{3t}^0 = \varepsilon_{4b}^0 = \varepsilon_D^0 = \varepsilon_F^0 \simeq 0.17479$.

the fourth band touch each other at two Dirac points ($\pm\mathbf{k}_D$) with the energy (ε_D^0) which are the same as the tops of the third band (ε_{3t}^0) at $\mathbf{k} = \pm\mathbf{k}_{3t}$ and the bottoms of the fourth band (ε_{4b}^0) at $\mathbf{k} = \pm\mathbf{k}_{4b}$. The Fermi energy for the 3/4-filled (ε_F^0) is equal to ε_D^0, as shown in Fig. 11(a). This is supported from the first-principles band calculations by Kino and Miyazaki [51] and Alemany, Pouget, and Canadell [52]. It has been also known that the system is semimetallic at $P < 3.0$, where the Fermi surfaces are shown in Fig. 12. There are a hole pocket centered at $\mathbf{k}_{3t} = (0,\pi/b)$ and an electron pocket enclosing two Dirac points at $\mathbf{k} = (\pi/a,0)$. An electron pocket separates into two small electron pockets with the same area at $0.2 \lesssim P < 3.0$, as shown in Fig. 12.

We find interesting features of the third and fourth bands near the Fermi energy at $P \lesssim 3.0$. When $P < 2.3$, the Dirac cones are overtilted (for example, see Fig. 2 at $P = 0$), where ε_D^0 at $\mathbf{k}_D$ is larger than ε_{4b}^0 at $\mathbf{k}_{4b}$, which can be also seen in

Fig. 11(a). As p increases, $\mathbf{k}_{4b}$ and $\mathbf{k}_D$ move on the k_x-k_y plane and these wave numbers coincide at $P = 2.3$, as shown in Fig. 11(b). In this case we have to take into account higher order terms in energy dispersion at Dirac points, and the quadratic term in one direction makes ε_D^0 at the Dirac points to be the global minima of the fourth band [i.e., $\varepsilon_D^0 = \varepsilon_{4b}^0$; see Figs. 11(a) and 13]. On the other hand, ε_D^0 is not the local maximum of the third band, as shown in Fig. 13. At $P = 2.3$ the Dirac cones are critically tilted, which have a quadratic dispersion in one direction and linear dispersions in the other three directions. In this sense, we name the Dirac cones at $P = 2.3$ "three-quarter" Dirac cones and these touching points "three-quarter" Dirac points [$\pm\mathbf{k}_{tq} = \pm\mathbf{k}_D \simeq \pm(0.6270\pi/a, 0.4058\pi/b)$]. At $2.3 < P < 3.0$, ε_D^0 is the global minimum of the fourth band and the local maximum of the third band, as shown in Fig. 14(a)
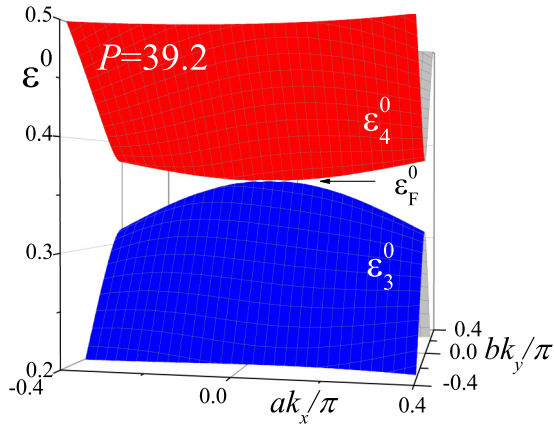
FIG. 5. The third and fourth energy bands at $P = 39.2$. Two Dirac points merge at the Γ point.

at $P = 2.75$. At $P = 3.0$ the Dirac cone of the third band is almost laid, as shown in Figs. 3 and 14(b). Since the density of states near the Dirac points is proportional to $|\varepsilon^0 - \varepsilon_D^0|$ and the density of states near the global maximum of the third band is constant, we obtain at $2.3 < P < P_c = 3.0$ (see Appendix E)

$$\varepsilon_{3t}^0 - \varepsilon_F^0 \propto (P_c - P)^2, \tag{5}$$

which can be seen in Fig. 11(a).

At $3.0 < P < 39.2$, ε_D^0 is the global minimum of the fourth band and the global maximum of the third band; i.e., massless Dirac fermions are realized [3], as shown in Fig. 14(c) at $P = 3.5$ and Fig. 4 at $P = 5.0$. Three bands from the bottom are fully occupied and the fourth band is completely empty at $T = 0$.

Two Dirac points move and merge [13] at a semi-Dirac point (Γ point) at $P = 39.2$, as shown in Fig. 5. At $P > 39.2$, the energy gap becomes finite [13]. The top of the third band and the bottom of the fourth band are approximately given by the anisotropic parabolic bands [12,53], where massive Dirac fermions are realized, as shown in Fig. 6 at $P = 50$.
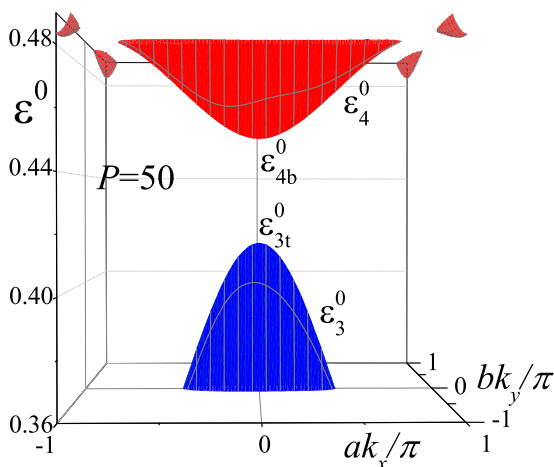

FIG. 6. The third and fourth energy bands at $P = 50$. The top of the third band and the bottom of the fourth band are obtained as $\varepsilon_{3t}^0 \simeq 0.41471$ and $\varepsilon_{4b}^0 \simeq 0.45378$, respectively.
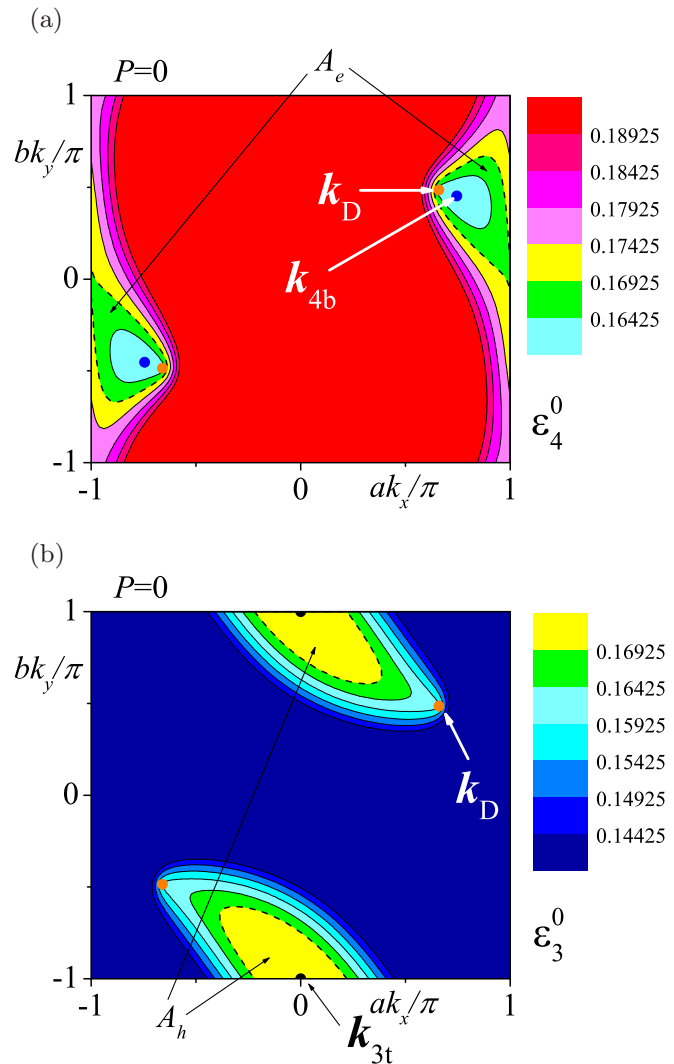

FIG. 7. Contour plots of the fourth band (a) and the third band (b) at $P = 0$. The electron and hole pockets depicted by dotted black lines are the Fermi surface at $\varepsilon = \varepsilon_F^0 \simeq 0.16925$. The areas of these electron and hole pockets (A_e and A_h) are about 0.0715 of the area of the first Brillouin zone (A_{BZ}). The third and the fourth bands touch at two Dirac points (orange points), $\pm \mathbf{k}_D \simeq \pm(0.6600\pi/a, 0.4854\pi/b)$. The third band has a top energy (ε_{3t}^0) at a black point, $\mathbf{k}_{3t} = (0, \pi/b)$. The fourth band has the bottom energy (ε_{4b}^0) at two blue points, $\pm \mathbf{k}_{4b} = \pm(0.7455\pi/a, 0.4530\pi/b)$.

Based on these results, we give a schematic phase diagram as a function of P in Fig. 15. The semimetallic state is divided to two phases (I and II) at $P < 2.3$ and at $2.3 < P < 3.0$.

III. ENERGY IN MAGNETIC FIELD

We obtain the energy in the magnetic field as eigenvalues of a $4q \times 4q$ matrix, when the magnetic flux in the unit cell (Φ) is a rational number in the unit of the flux quantum ($\phi_0 = 2\pi\hbar c/e \simeq 4.14 \times 10^{-15}$ T m^2), i.e.,

$$h = \frac{\Phi}{\phi_0} = \frac{p}{q}, \tag{6}$$

where p and q are integers. This is explained in Appendix D. Hereafter, we represent the magnetic field by h. Since
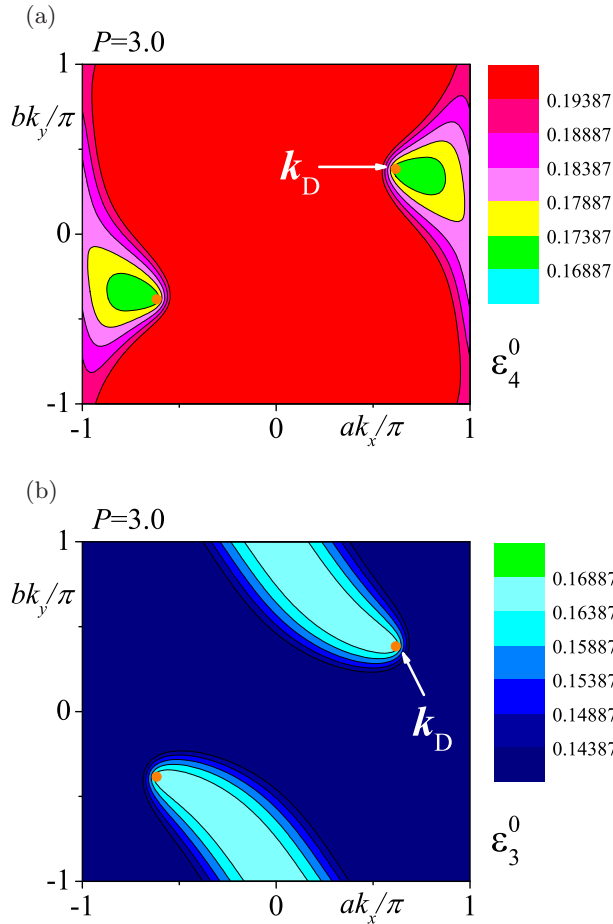
FIG. 8. Contour plots of the fourth band (a) and the third band (b) at $P = 3.0$. The third band and fourth band touch at two orange points, $\pm \mathbf{k}_D \simeq \pm(0.6169\pi/a, 0.3835\pi/b)$.

FIG. 9. Contour plots of fourth band (a) and the third band (b) at $P = 5.0$.

$a \simeq 9.211$ Å and $b \simeq 10.85$ Å in α-(BEDT-TTF)$_2$I$_3$ [1], $h = 1$ corresponds to $H \simeq 4.14 \times 10^3$ T. The lowest magnetic field studied in this paper is $h = 2/1901$, i.e., $H \simeq 4.36$ T.

We show the energies as a function of h (the Hofstadter butterfly diagrams) at $P = 0$, 5.0, and 39.2 in Fig. 16. The energies near the Fermi energy at $P = 0$, 3.0, 5.0, and 39.2 are shown in Fig. 17. If q is small, each band may be broadened, and we have to consider the **k** dependence of the energy. If q is large, the widths of $4q$ bands become narrow, and the **k** dependencies of each band can be neglected, as long as the contour line of the energy in the wave-number space is closed at $h = 0$. When the contour line of the energy in the wave-number space is open, which is the case for $\varepsilon^0 \simeq 0.175$ at $P = 0$ [Fig. 7(a)], we have to consider the **k** dependencies in each band. In fact, the energies are broadening above $\varepsilon \gtrsim 0.175$, as shown in Figs. 17(a) and 18. There are $4q$ bands, some of which may overlap each other.

When the chemical potential is in the energy gap in the magnetic field, Hall conductance is quantized. The quantized value is obtained as a first Chern number [54–56]. It is also given as a solution of the Diophantine equation [55,56],

$$r = qs_r + pt_r, \qquad (7)$$

where p and q are given in Eq. (6), r is the number of energy bands below the chemical potential, and s_r and t_r are integers
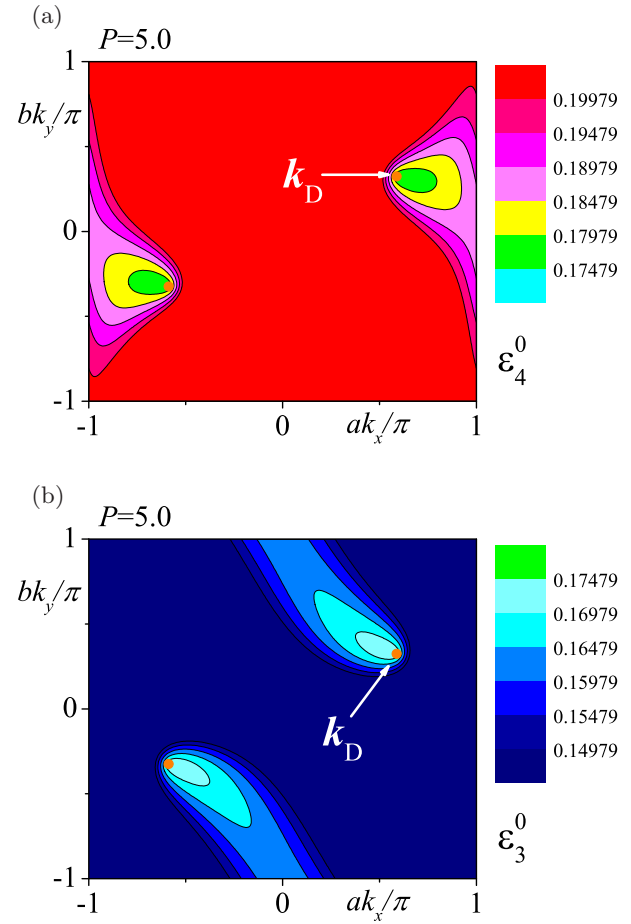
obtained in this Diophantine equation. Although s_r and t_r are not given uniquely from Eq. (7), we can uniquely assign integers (s_r and t_r) in the energy gaps in the Hofstadter butterfly diagrams. In this system, s_r and t_r are shown in Fig. 17.

A. Semimetallic state I at $P < 2.3$

The energy near the Fermi energy at $P = 0$ at the relatively low magnetic field is shown in Fig. 18. We fit the energy levels for the fourth band starting from $h = 0$ and $\varepsilon = \varepsilon^0_{4b}$ as

$$\varepsilon_n - \varepsilon^0_{4b} \propto h^{\delta_n}, \qquad (8)$$

where $\delta_n = 0.9$, 0.89, and 0.86, as shown in Fig. 18. Those Landau levels are not linear in h. If a fitting could be performed at very low magnetic fields, $\delta_n = 1$ would be obtained due to the parabolic dispersion of the fourth band around ε^0_{4b} [see Fig. 2(c)]. However, h is not sufficiently low in Fig. 18. Therefore, the deviation from the parabolic dispersion around ε^0_{4b} makes the fitting parameter δ_n to be smaller than 1.

Two upward-sloping Landau levels starting from ε^0_{4b} in Fig. 18 are almost degenerate at low h and below ε^0_F. They are smoothly separated near ε^0_F. The lift of the degeneracy of the Landau levels around ε^0_F (Fig. 12) is understood semiclassically as follows. The fourth band has minima ε^0_{4b} at $\pm \mathbf{k}_{4b}$ [see Fig. 2 and Fig. 7(a)]. When the energy is located between ε^0_{4b} and the
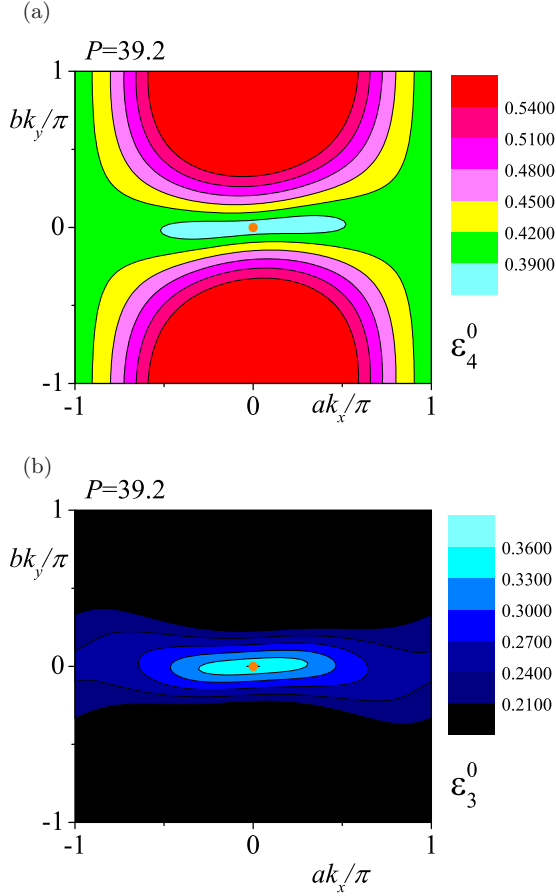
FIG. 10. Contour plots of the fourth band (a) and the third band (b) at $P = 39.2$, where $\varepsilon_F^0 \simeq 0.36165$. Two Dirac points merge at a Γ point [orange point, $(ak_x/\pi, bk_y/\pi) = (0,0)$].

energy at the saddle point $[\mathbf{k} = (\pi/a, 0)]$ of the fourth band, as seen in Fig. 7(a), the contour line of energy in the fourth band consists of two closed regions (two electron pockets). Two minima are considered to be independent, resulting in the degenerated Landau levels. When the energy is larger than that at the saddle point, the contour line of energy in the fourth band is one closed loop, making no degeneracy of Landau levels. The energy at the saddle point is close to ε_F^0. A similar situation has been studied by Montambaux, Piechon, Fuchs, and Goerbig [12,53].

The Landau levels for the third band are fitted by

$$\varepsilon_n = -0.12\left(n + \tfrac{1}{2}\right)h + \varepsilon_{3t}^0, \; n = 0, 1, 2, \ldots, \quad (9)$$

which are depicted by black broken lines in Fig. 18. These Landau levels are understood as the Landau quantization for a free hole pocket centered at $\mathbf{k} = \mathbf{k}_{3t}$.

B. Three-quarter Dirac points at *P* = 2.3

In order to write the energy near three-quarter Dirac points at $P = 2.3$ we take a model (see Appendix F) as

$$\mathcal{H}_{tqD}^0 = \begin{pmatrix} -w_x q_x + \alpha_2' q_x^2 & w_x q_x + \alpha_2'' q_x^2 - i w_y q_y \\ w_x q_x + \alpha_2'' q_x^2 + i w_y q_y & -w_x q_x + \alpha_2' q_x^2 \end{pmatrix},$$
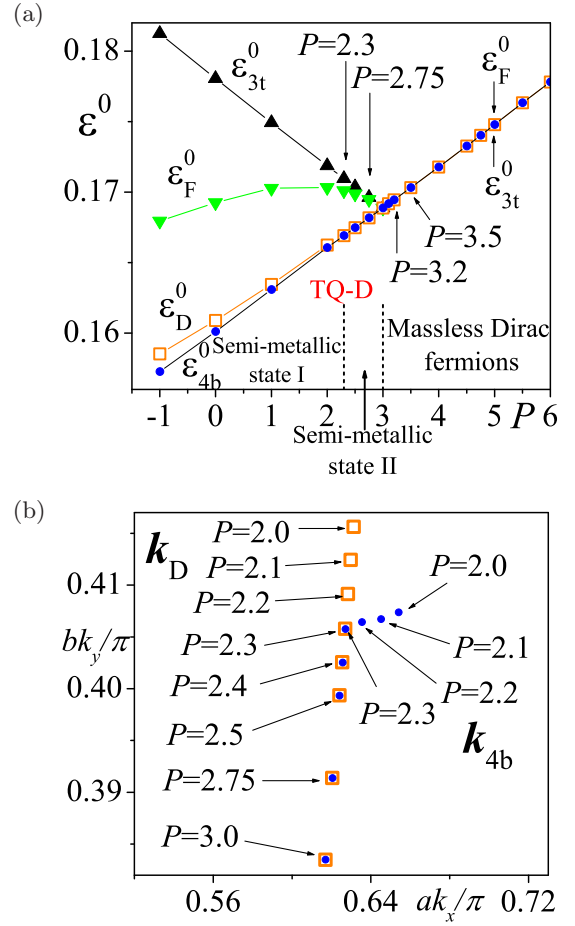
$$(10)$$

FIG. 11. (a) Pressure dependencies of the energies at the Dirac point (ε_D^0, orange open squares), the top of the third band (ε_{3t}^0, black filled triangles), the bottom of the fourth band (ε_{4b}^0, blue filled circles), and the Fermi energy for the 3/4 filled (ε_F^0, green filled inverse triangles). All of the energies ε_{3t}^0, ε_{4b}^0, ε_D^0, and ε_F^0 become the same values at $P \gtrsim 3.0$. At $P = 2.3$ the Dirac points become three-quarter Dirac points (TQ-D). (b) Pressure dependencies of the wave numbers of the Dirac point ($\mathbf{k}_D$, orange open squares) and the bottom of the fourth band ($\mathbf{k}_{4b}$, blue filled circles).

where $\mathbf{q} = 0$ corresponds to $\mathbf{k}_{tq}$. The eigenvalues are obtained as

$$\varepsilon_{tqD\pm}^0(\mathbf{q}) = -w_x q_x + \alpha_2' q_x^2 \pm \sqrt{\left(w_x q_x + \alpha_2'' q_x^2\right)^2 + (w_y q_y)^2}.$$

$$(11)$$

The fourth band and the third band correspond to $\varepsilon_{tqD+}^0(\mathbf{q})$ and $\varepsilon_{tqD-}^0(\mathbf{q})$, respectively. The energy $\varepsilon_{tqD+}^0(\mathbf{q})$ around $\mathbf{q} = (0,0)$ is linear in three directions $\mathbf{q} = \pm(0, |q_y|)$ and $\mathbf{q} = (-|q_x|, 0)$ but quadratic in one direction $\mathbf{q} = (|q_x|, 0)$, when $w_x > 0$. Therefore this model represents the dispersion near a three-quarter Dirac point, as shown in Fig. 13. We obtain the area enclosed by the constant energy line at $\varepsilon_{tqD+}^0(\mathbf{q}) = \varepsilon$ to be

$$A(\varepsilon) \simeq \frac{\sqrt{2w_x}\,\pi}{4w_y} \alpha_2^{-\frac{3}{4}} \varepsilon^{\frac{5}{4}}, \quad (12)$$

where $\alpha_2 = \alpha_2' + \alpha_2''$, in the limit of $\varepsilon \to +0$. Equation (12) is derived in Appendix F. By using Eq. (12) and the semiclassical quantization rule of Eq. (A1) with $\gamma = 0$, we
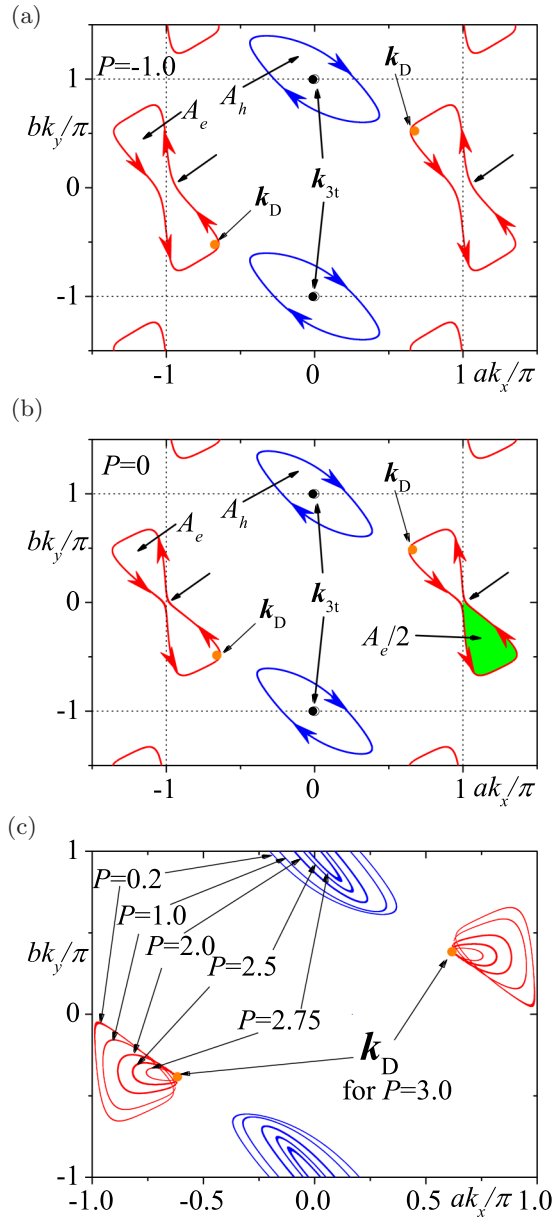
(a)

(b)

(c)

FIG. 12. Fermi surfaces at $P = -1.0$ (a) and $P = 0$ (b) in the extended zone, where arrows indicate the direction of the orbital motion for electrons in the magnetic field (clockwise for hole pockets and counterclockwise for electron pockets). In (b), a green area is half of A_e. In (c), the Fermi surfaces for $P = 0.2, 1.0, 2.0, 2.5$, and 2.75 in the first Brillouin zone are shown, where orange points are for $\mathbf{k}_D$ at $P = -1.0, 0$, and 3.0 and black points are for $\mathbf{k}_{3t}$ at $P = -1.0$ and 0. The wave number, $\mathbf{k}_{3t}$, stays at $(0, \pi/b)$ at $P < 3.0$. We obtain $A_e = A_h \simeq 0.0903$ at $P = -1.0$, $A_e = A_h \simeq 0.0715$ at $P = 0$, and $A_h \simeq 0.0479$ at $P = 1.0$ in the unit of the area of the Brillouin zone, where A_e and A_h are the areas of an electron pocket and a hole pocket, respectively. The ratio of cyclotron masses for an electron pocket and a hole pocket (m_e/m_h) are about 0.71, 0.63, and 0.61 at $P = -1.0$, 0, and 1.0.

obtain semiclassically the Landau levels for three-quarter Dirac cones in the fourth band as

$$\varepsilon_n^{\text{(three-quarter Dirac)}} - \varepsilon_D^0 \propto (nh)^{\frac{4}{5}}. \tag{13}$$
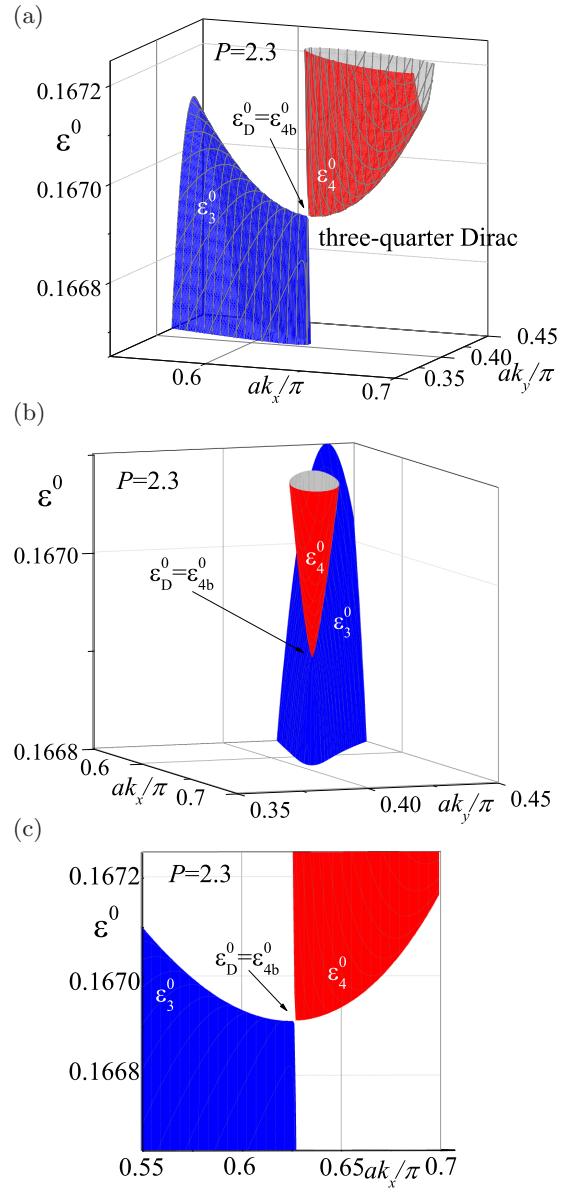

(a)

(b)

(c)

FIG. 13. Energy dispersion near the Dirac point (three-quarter Dirac point) at $P = 2.3$ from three different viewpoints [(a), (b), and (c)]. In (c), $0.35\pi/b \leqslant k_y < 0.45\pi/b$.

The Landau levels starting from $\varepsilon = \varepsilon_D^0$ at $h = 0$ are fitted as

$$\varepsilon_0 = \varepsilon_D^0, \tag{14}$$

$$\varepsilon_1 = 0.158 h^{0.8} + \varepsilon_D^0, \tag{15}$$

$$\varepsilon_2 = 0.158 (2h)^{0.8} + \varepsilon_D^0, \tag{16}$$

$$\varepsilon_3 = 0.158 (3h)^{0.8} + \varepsilon_D^0, \tag{17}$$

as shown in Fig. 19(a), which are consistent with the semiclassical quantization of the energy [Eq. (13)]. The level ε_0 is not as clearly seen as ε_1, ε_2, and ε_3. The reason for the ambiguous energy levels of $n = 0$ in Fig. 19(a) might
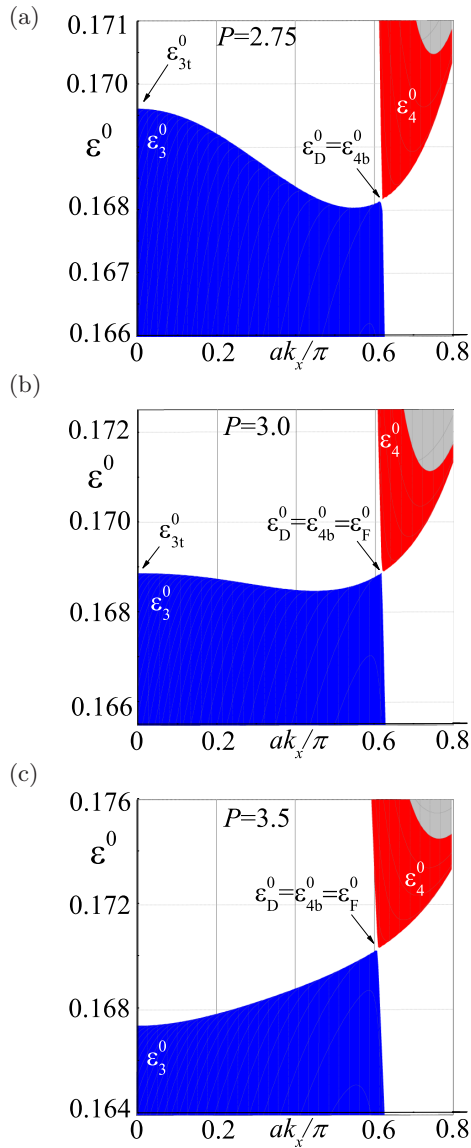
FIG. 14. Energy dispersion near the Dirac point from a viewpoint along the k_y axis at $P = 2.75$ (a) and $P = 3.0$ (b), where $0.3\pi/b \leqslant k_y < \pi/b$, and at $P = 3.5$ (c), where $0.25\pi/b \leqslant k_y < \pi/b$.

be the mixing of the $n = 0$ Landau level for the fourth band and the Landau levels for the third band with a negligible tunneling barrier at three-quarter Dirac points.
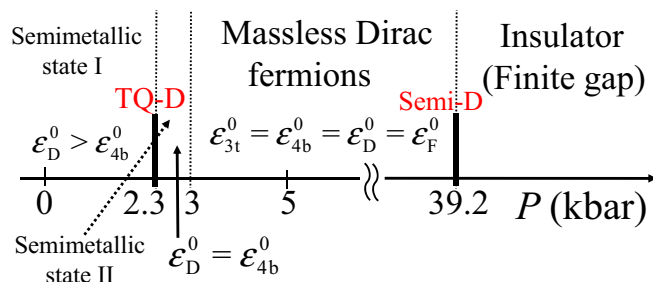

FIG. 15. A schematic phase diagram as a function of P. In semimetallic phase I ($P < 2.3$), $\varepsilon_D^0 > \varepsilon_{4b}^0$. In semimetallic phase II ($2.3 < P < 3.0$), $\varepsilon_D^0 = \varepsilon_{4b}^0$.
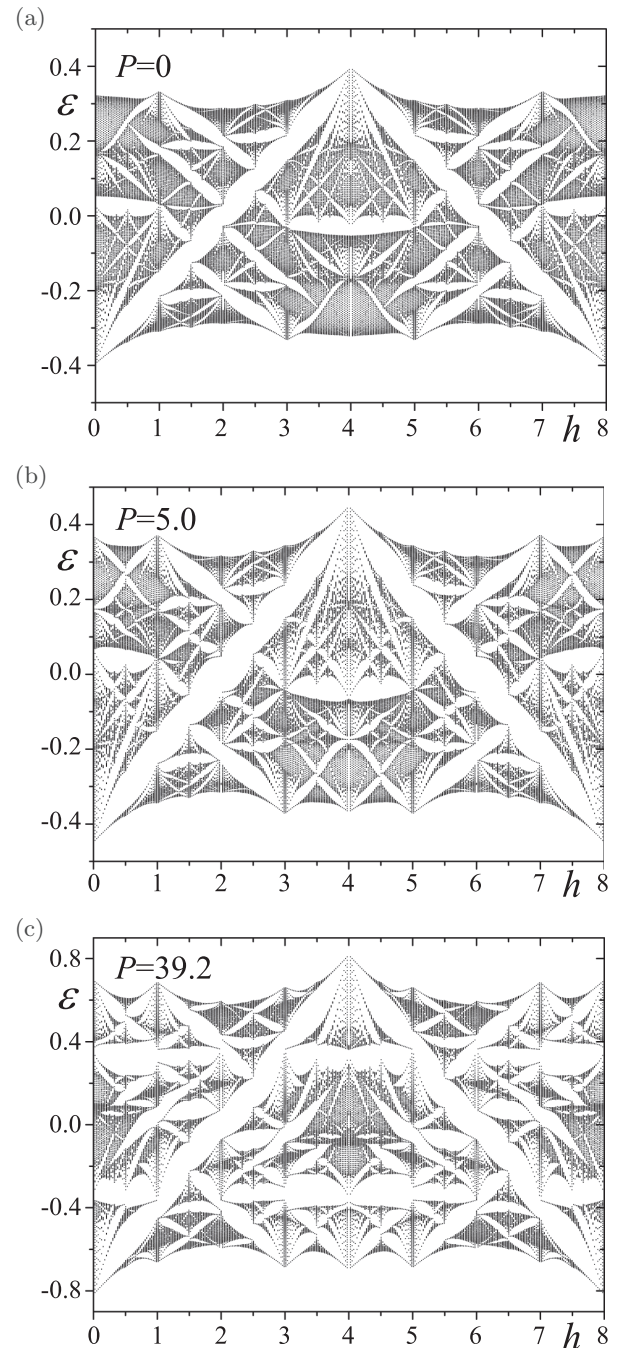

FIG. 16. Energies as a function of h for $P = 0$ (a), $P = 5.0$ (b), and $P = 39.2$ (c). We take $h = p/q$ with $q = 79$ and $p = 2m$, where $m = 1, 2, 3, \ldots, 4q$.

When the magnetic field is low, the Landau levels for the third band are approximately written by

$$\varepsilon_n = -0.054\left(n + \tfrac{1}{2}\right)h + \varepsilon_{3t}^0, \; n = 0, 1, 2, \quad (18)$$

which comes from a hole pocket centered at $\mathbf{k} = \mathbf{k}_{3t}$.

C. Semimetallic state II at $2.3 < P < 3.0$

At $2.3 < P < 3.0$, ε_D^0 is the global minimum of the fourth band but only the local maximum of the third band. The global

FIG. 18. Energies near the Fermi energy as a function of h at $P = 0$, where $\varepsilon_F^0 \simeq 0.16925$. We take $h = 2/q$ ($q = 200, 201, \ldots, 799, 800$).

At $P = 2.75$ the Landau levels for the fourth band are fitted by

$$\varepsilon_n - \varepsilon_D^0 \propto h^{0.73}, \qquad (19)$$

as shown in Fig. 19(b). The fitting parameter (the power of h) is obtained to be 0.73, which is different from 0.8 expected in the case of the three-quarter Dirac point at $P = 2.3$. The effect of the finite linear term in one direction, which is zero in the case of the three-quarter Dirac point, is not large enough to make the fitting parameter to be 0.5 in the region of the magnetic field in Fig. 19(b).

The Landau levels for the third band [Fig. 19(b)] are fitted by

$$\varepsilon_n = -0.033\left(n + \tfrac{1}{2}\right)h + \varepsilon_{3t}^0, \quad n = 0, 1, 2, \ldots, \qquad (20)$$

which is understood as the Landau quantization of a free hole pocket.

The energies as a function of a magnetic field are changed smoothly as a pressure P is changed in the semimetallic state II [Figs. 19(a)–19(c)]. The fitting parameters (the power in h) for the quantized energy in the fourth band are changed continuously from 4/5 (three-quarter Dirac point) to smaller values, while the quantized energies in the third band are well fitted by the Landau levels for a free hole band, as long as the quantized energy is larger than the energy at the Dirac point. The quantization of the energy of the third band at $P = 3.0$ is discussed in the following subsection.

D. At the critical pressure $P_c = 3.0$

The energy ε_{3t}^0 at $\mathbf{k}_{3t} = (0, \pi/a)$ is the same as ε_D^0 at $P = 3.0$ [see Figs. 11(a) and 14(b)]. Then the third band is almost constant at the line connecting ε_{3t}^0 and ε_D^0. We calculate the magnetic field dependence of the energy [Fig. 19(c)]. The log-log plot near the Fermi energy is shown in Fig. 20. The energies for the fourth band are fitted by

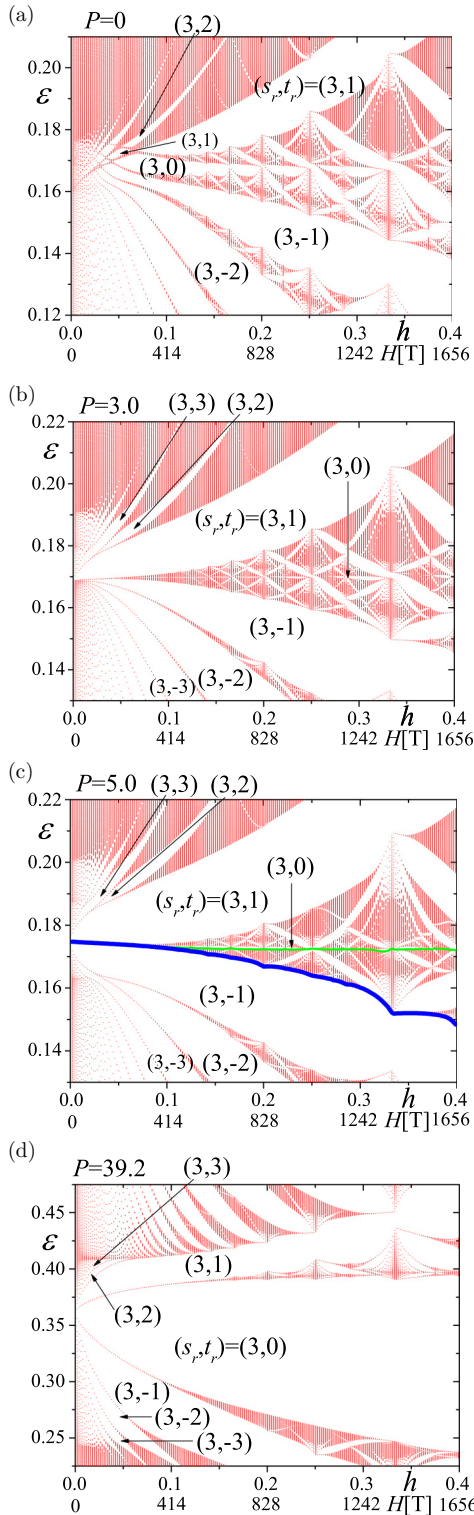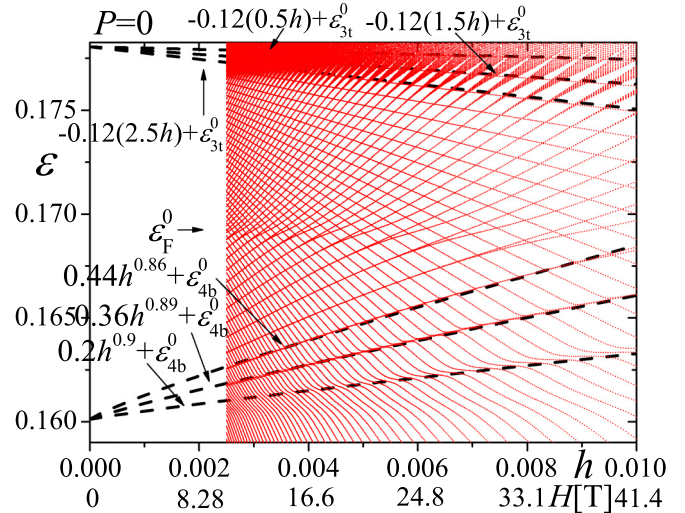$$\varepsilon_n - \varepsilon_F^0 \propto h^{0.7}. \qquad (21)$$

FIG. 17. Energies as a function of h for $P = 0$ (a), $P = 3.0$ (b), $P = 5.0$ (c), and $P = 39.2$ (d). We take $h = \frac{2m}{499}$ ($m = 1, 2, 3, \ldots, 99$) and $h = \frac{2(2m-1)}{998}$ ($m = 1, 2, 3, \ldots, 100$), namely, where $p/q = 2/998, 2/499, 6/998, 4/499, \ldots, 198/499, 398/998$.

maximum of the third band, ε_{3t}^0, is obtained at $\mathbf{k}_{3t} = (0, \pi/a)$. The Fermi energy, ε_F^0, is between ε_D^0 and ε_{3t}^0. We defined this state as semimetallic state II (see Fig. 15).
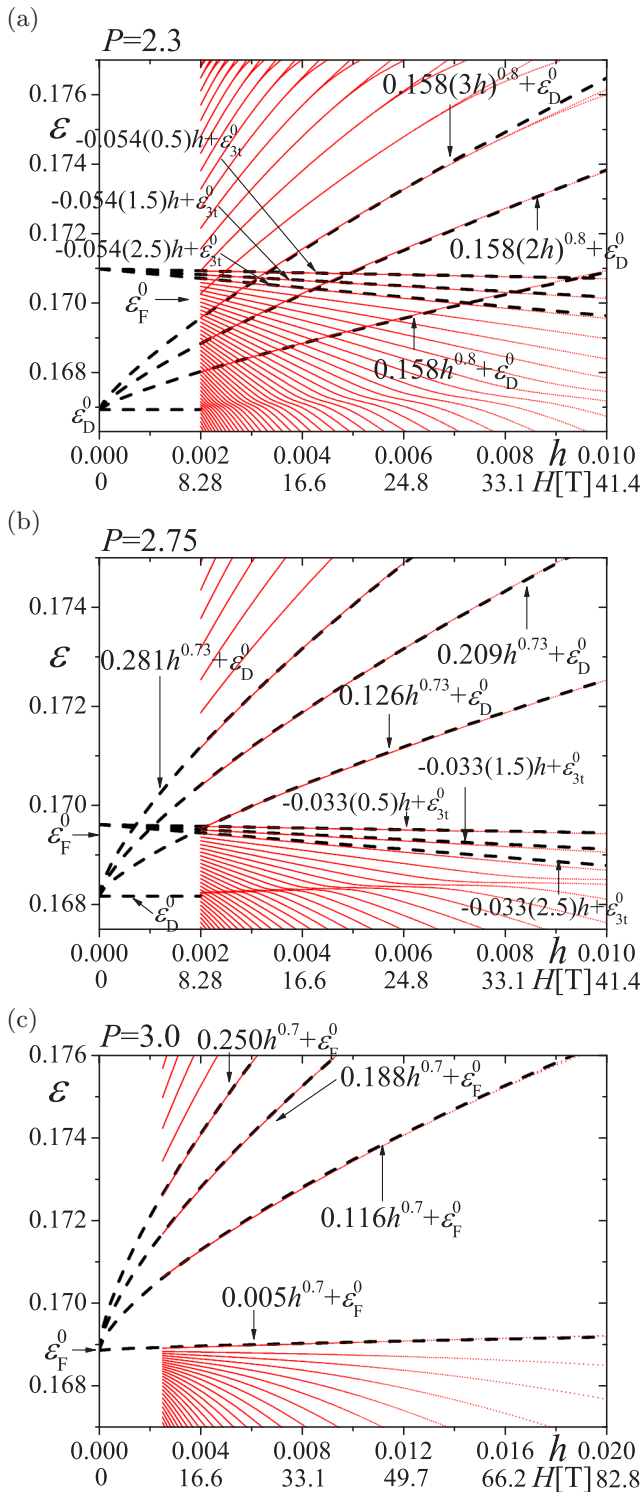
FIG. 19. Energies near the Fermi energy as a function of h for $P = 2.3$ (a), $P = 2.75$ (b), and $P = 3$ (c). We choose $p = 2$ and $200 \leqslant q \leqslant 1000$ ($q = 200, 201, \ldots, 999, 1000$) for (a) and (b) and $p = 2$ and $100 \leqslant q \leqslant 800$ ($q = 100, 101, \ldots, 799, 800$) for (c), respectively.

Equation (21) is obtained from a fitting at the intermediate magnetic field. If we could perform a fitting at the low magnetic field limit, we could obtain $\propto \sqrt{h}$.
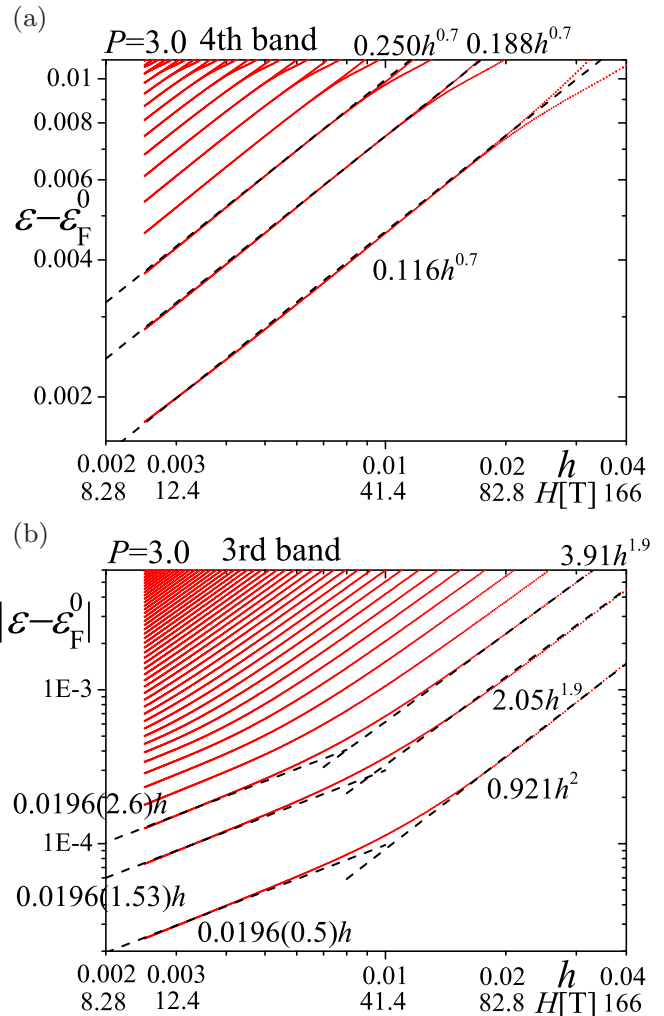

FIG. 20. The log-log plot of Fig. 19(c) at $P = 3.0$ at $0.025 \leqslant h \leqslant 0.04$ (10.4 T $\leqslant H \leqslant$ 166 T). (a) The energy larger than ε_F^0, which corresponds to the fourth band at $h = 0$ and (b) the energy smaller than ε_F^0, which corresponds to the third band at $h = 0$.

For the third band, the quantized energies below ε_F^0 are fitted by

$$\varepsilon_n = -0.0196\left(n + \tfrac{1}{2}\right)h + \varepsilon_F^0, \ n = 0, 1, 2 \qquad (22)$$

for $h \lesssim 0.005$ and

$$\varepsilon_F^0 - \varepsilon_n \propto h^2 \qquad (23)$$

for $h \gtrsim 0.01$ as shown in Fig. 20(b).

The magnetic field dependencies of Eqs. (22) and (23) can be understood as follows. When the magnetic field is weak ($h \lesssim 0.005$), the energy is quantized as the Landau levels for a free hole pocket around $\mathbf{k}_{3t}$. On the other hand, when $h \gtrsim 0.01$, we can neglect the small curvature around $\mathbf{k}_{3t}$ and very small regions of local maxima around $\pm\mathbf{k}_D$. Then, an almost flat ridge from $\mathbf{k}_D$ to $-\mathbf{k}_D$ via $\mathbf{k}_{3t}$ is quantized in the intermediate value of the magnetic field. We consider a model for this situation as

$$\mathcal{H}^{0,\mathrm{ridge}} = \frac{1}{2m}p_x^2 + V(p_y), \qquad (24)$$

where

$$V(p_y) = \begin{cases} 0, & \text{if } |p_y| < p_0, \\ \infty, & \text{otherwise,} \end{cases} \qquad (25)$$

where p_0 is the length of the ridge, i.e., $p_0 \simeq 2\hbar|\mathbf{k}_D - \mathbf{k}_{3t}|$. In the presence of the magnetic field, $\mathbf{p}$ is replaced by

$$-i\hbar\nabla - \frac{e}{c}\mathbf{A}, \qquad (26)$$

where $\mathbf{A}$ is vector potential, and we take

$$\mathbf{A} = (0, Hx, 0). \qquad (27)$$

Then the eigenvalue $\varepsilon^{\text{ridge}}$ is obtained by the equation,

$$\left\{\frac{-\hbar^2}{2m}\frac{\partial^2}{\partial x^2} + V\left(-i\hbar\frac{\partial}{\partial y} - \frac{e}{c}Hx\right)\right\}\Psi(x,y) = \varepsilon^{\text{ridge}}\Psi(x,y). \qquad (28)$$

The eigenstates are obtained as

$$\Psi(x,y) = e^{ik_y y}\psi(x), \qquad (29)$$

where $\psi(x)$ is a solution of

$$\left\{\frac{-\hbar^2}{2m}\frac{d^2}{dx^2} + V\left(\hbar k_y - \frac{e}{c}Hx\right)\right\}\psi(x) = \varepsilon^{\text{ridge}}\psi(x). \qquad (30)$$

Since Eq. (30) is the Schrödinger equation for the one-dimensional quantum well with width $2c/(eHp_0)$, the eigenvalue is quantized as

$$\varepsilon_n^{\text{ridge}} = \frac{\hbar\pi^2 p_0^2 e^2}{8mc^2}(nH)^2, \qquad (31)$$

where $n = 1, 2, 3, \ldots$. In spite of the simple approximation [Eqs. (24) and (25)], we can explain the h^2 dependence seen in Fig. 20(b).

E. Dirac fermions system at $3.0 \leqslant P < 39.2$, semi-Dirac fermions at $P = 39.2$, and massive Dirac fermions system at $P > 39.2$

We show the energies near the Fermi energy as a function of h at $P = 5.0, 39.2$, and 50 in Fig. 21 at the low magnetic field. The magnetic field dependencies of the energies at $P = 5.0$ are fitted by

$$\varepsilon_n = \begin{cases} 0.064\sqrt{nh} + \varepsilon_F^0, & n = 0, 1, 2, 3, 4, \\ -0.066\sqrt{|n|h} + \varepsilon_F^0, & n = 0, -1, -2, -3, -4, \end{cases} \qquad (32)$$

which is expected in the system with massless Dirac fermions [Eq. (2)].

At $P = 39.2$ the dispersion is parabolic in two directions and linear in the other two directions at the semi-Dirac point, as shown in Fig. 5. The magnetic field dependencies of the energies near ε_F^0 at the low magnetic field are fitted by

$$\varepsilon_n = \begin{cases} 0.39 g_+(n)\left[\left(n+\tfrac{1}{2}\right)h\right]^{\frac{2}{3}} + \varepsilon_F^0, & n = 0, 1, 2, \\ -0.58 g_-(n)\left[\left|n+\tfrac{1}{2}\right|h\right]^{\frac{2}{3}} + \varepsilon_F^0, & n = 0, -1, -2, \end{cases} \qquad (33)$$

where $g_+(0) \simeq 0.769$, $g_-(0) \simeq 0.897$, and $g(n) = 1$ for $|n| = 1, 2$, as shown in Fig. 21(b). This magnetic field dependence is expected in the system with the semi-Dirac point [Eq. (3)].
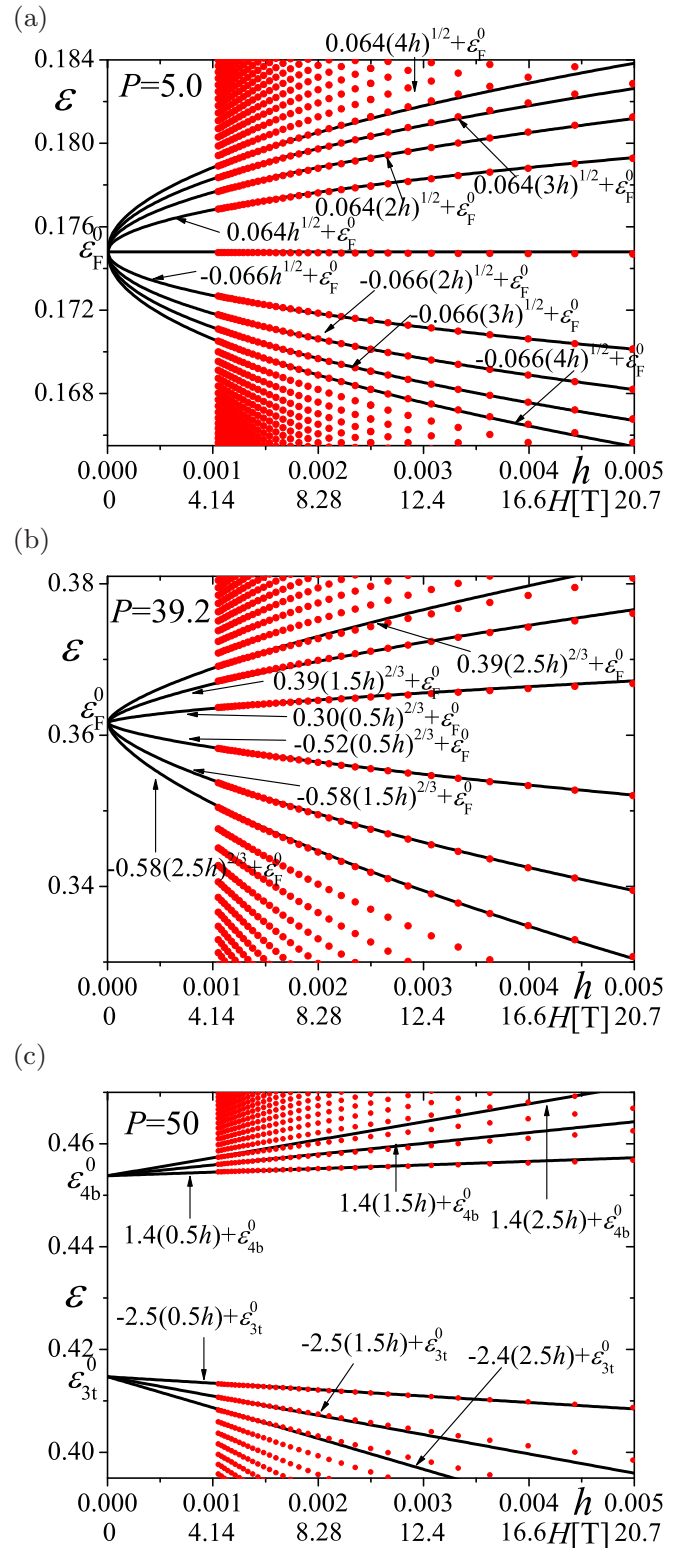

FIG. 21. Energies as a function of h for $P = 5.0$ (a), $P = 39.2$ (b), and $P = 50$ (c). We choose $p = 2$ and $q = 1901, 1851, 1801, \ldots, 451, 401$.

At $P = 50$, where massive Dirac fermions are realized, the Landau levels are fitted by

$$\varepsilon_n = -2.5\left(n+\tfrac{1}{2}\right)h + \varepsilon_{3t}^0, \qquad (34)$$

$$\varepsilon_n = 1.4\left(n + \tfrac{1}{2}\right)h + \varepsilon_{4b}^0, \tag{35}$$

where $n = 0, 1, 2$. Equations (34) and (35) are due to the anisotropic parabolic bands.

IV. TOTAL ENERGY, MAGNETIZATION, AND DE HAAS–VAN ALPHEN OSCILLATION

In this section we study the total energy and the magnetization. It has been known [15] that the total energy and the magnetization as a function of the magnetic field depend on whether we fix the chemical potential (μ, i.e., grand canonical ensemble) or the electron number (N, or equivalently electron filling $\nu = N/N_s$, where N_s is the site number, i.e., canonical ensemble).

In the case of fixed μ, the thermodynamic potential (Ω) per sites at the temperature T is calculated as

$$\Omega = -\frac{k_B T}{4q N_k} \sum_{i=1}^{4q} \sum_{\mathbf{k}} \ln\left\{\exp\left(\frac{\mu - \varepsilon(i,\mathbf{k})}{k_B T}\right) + 1\right\}, \tag{36}$$

where k_B is the Boltzmann constant, N_k is the number of $\mathbf{k}$ points taken in the magnetic Brillouin zone, $4q$ is the number of bands in the presence of the magnetic field, and $\varepsilon(i,\mathbf{k})$ are the eigenvalues of the $4q \times 4q$ matrix in Eq. (D11). The site number, N_s, is given by $N_s = 4q N_k$. At $T = 0$, Ω becomes the total energy for the fixed μ,

$$E_\mu = \frac{1}{4q N_k} \sum_{\varepsilon(i,\mathbf{k}) \leqslant \mu} [\varepsilon(i,\mathbf{k}) - \mu]. \tag{37}$$

If the system is isolated from the reservoir of electrons, electron number (or electron filling ν) is conserved and the chemical potential changes depending on the magnetic field. Although it has been known that the magnetic field dependence of μ is negligibly small if we consider the effects of the three-dimensionality, thermal broadening, compensated metals, electron or hole reservoirs, etc. [30,31,57–64], the magnetic field dependence of μ cannot be neglected in two-dimensional systems in general. The chemical potential μ as a function of the magnetic field with fixed ν should be obtained by the solution of the equation,

$$\nu = \frac{1}{4q N_k} \sum_{i=1}^{4q} \sum_{\mathbf{k}} \frac{1}{\exp\left(\frac{\varepsilon(i,\mathbf{k}) - \mu}{k_B T}\right) + 1}, \tag{38}$$

where we take $\nu = 3/4$ in this study. Using the magnetic-field-dependent μ, the Helmholtz free energy (F) per sites at T is calculated as

$$F = -\frac{k_B T}{4q N_k} \sum_{i=1}^{4q} \sum_{\mathbf{k}} \ln\left\{\exp\left(\frac{\mu - \varepsilon(i,\mathbf{k})}{k_B T}\right) + 1\right\} + \mu\nu. \tag{39}$$

At $T = 0$ it becomes the total energy with fixed ν,

$$E_\nu = \frac{1}{4q N_k} \sum_{\varepsilon(i,\mathbf{k}) \leqslant \mu} \varepsilon(i,\mathbf{k}). \tag{40}$$

In this paper we study the systems with fixed chemical potential and fixed electron number at $T = 0$. We show E_ν

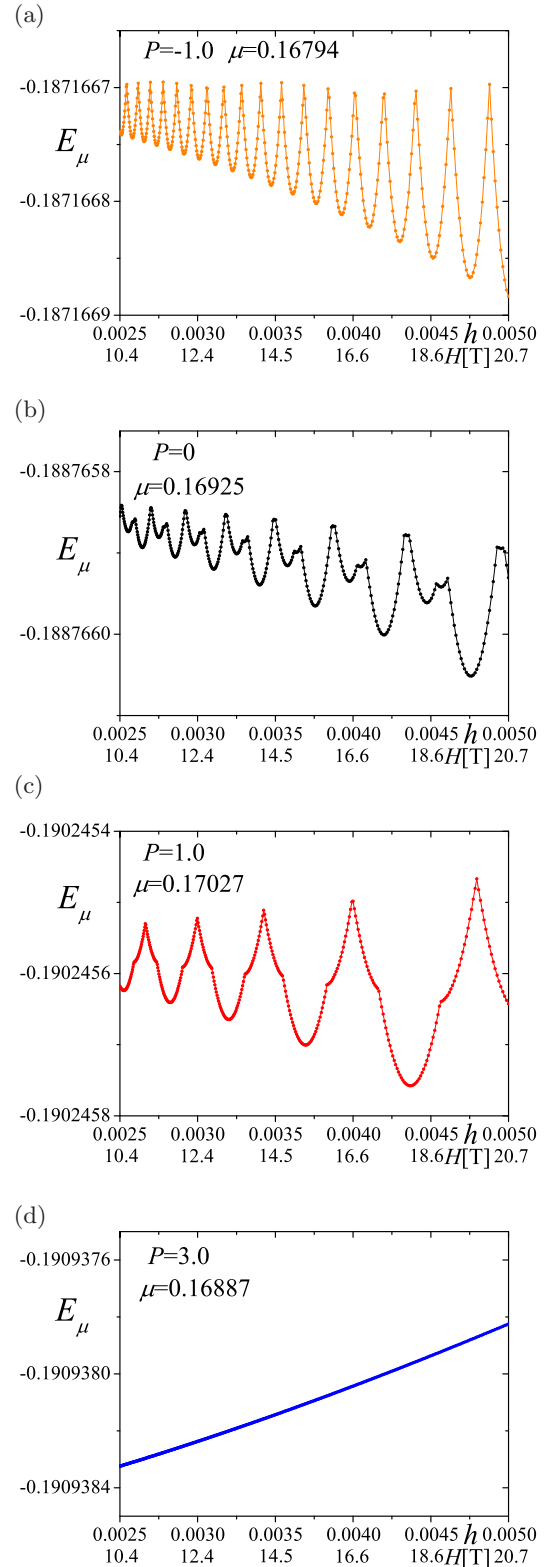FIG. 22. Total energies as a function of h at $P = -1.0$ (a), $P = 0$ (b), $P = 1.0$ (c), and $P = 3.0$ (d) with the fixed $\mu = \varepsilon_F^0$. The same values of $h = p/q$ are used as those in Fig. 29.

and E_μ at $P = -1.0, 0, 1.0$, and 3.0 for the low magnetic field in Figs. 22 and 23 and those for the high magnetic field at $P = -1.0, 0, 1.0, 3.0, 4.0, 5.0$, and 39.2 in Figs. 24 and 25. We
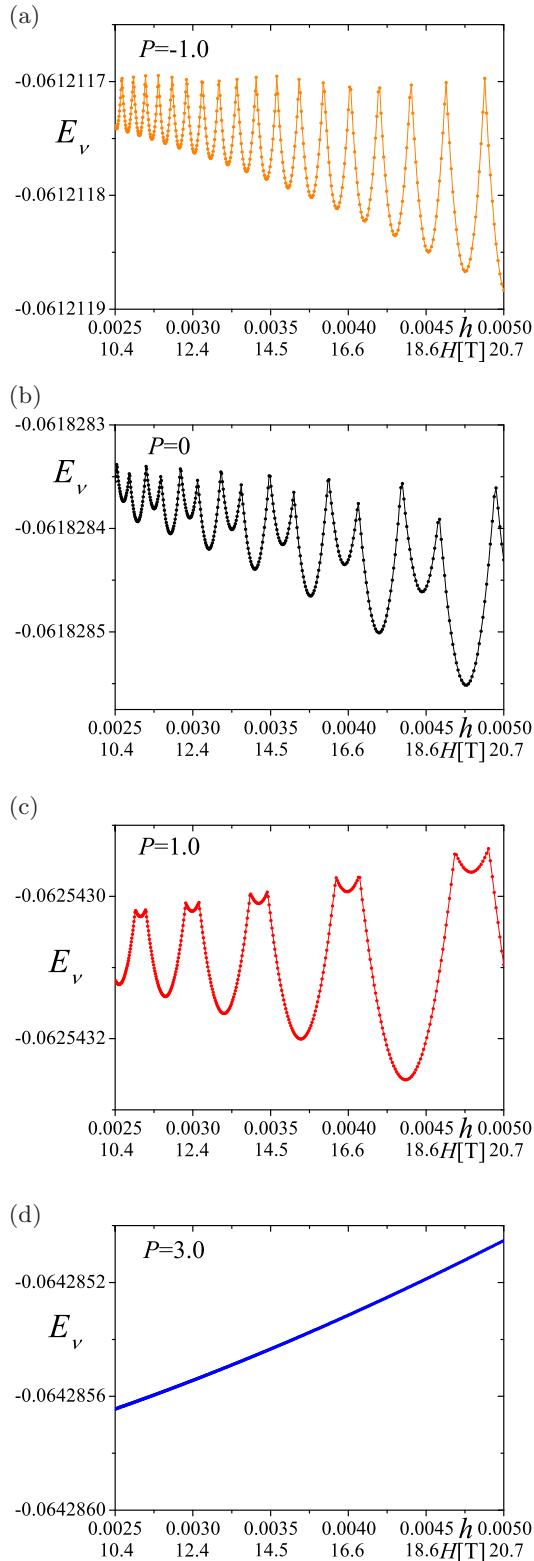
FIG. 23. Total energies as a function of h at $P = -1.0$ (a), $P = 0$ (b), $P = 1.0$ (c), and $P = 3$ (d) with the fixed $\nu = 3/4$. The same values of $h = p/q$ are used as those in Fig. 29.

FIG. 24. Total energies as a function of h at $P = -1.0$ (a), $P = 0$ (b), and $P = 1.0$ (c). We take $h = \frac{2m}{499}$ ($m = 1,2,3,\ldots,99$), $h = \frac{2(2m-1)}{998}$ ($m = 1,2,3,\ldots,100$), and $h = \frac{32}{q}$ ($q = 173,175,\ldots,355$).

The magnetizations are obtained for fixed μ and for fixed ν by

$$M_\nu = -\frac{\partial E_\nu}{\partial h}, \tag{41}$$

$$M_\mu = -\frac{\partial E_\mu}{\partial h}, \tag{42}$$

respectively, where the derivative with respect to h is calculated by the numerical differentiation. The magnetizations (M_ν and M_μ), calculated from E_ν and E_μ in Figs. 22–25, are shown in Figs. 26–28.

have checked that if q is large enough as taken in the present study, the wave-number dependence of the eigenvalues $\varepsilon(i,\mathbf{k})$ is very small and we can take $N_k = 1$.
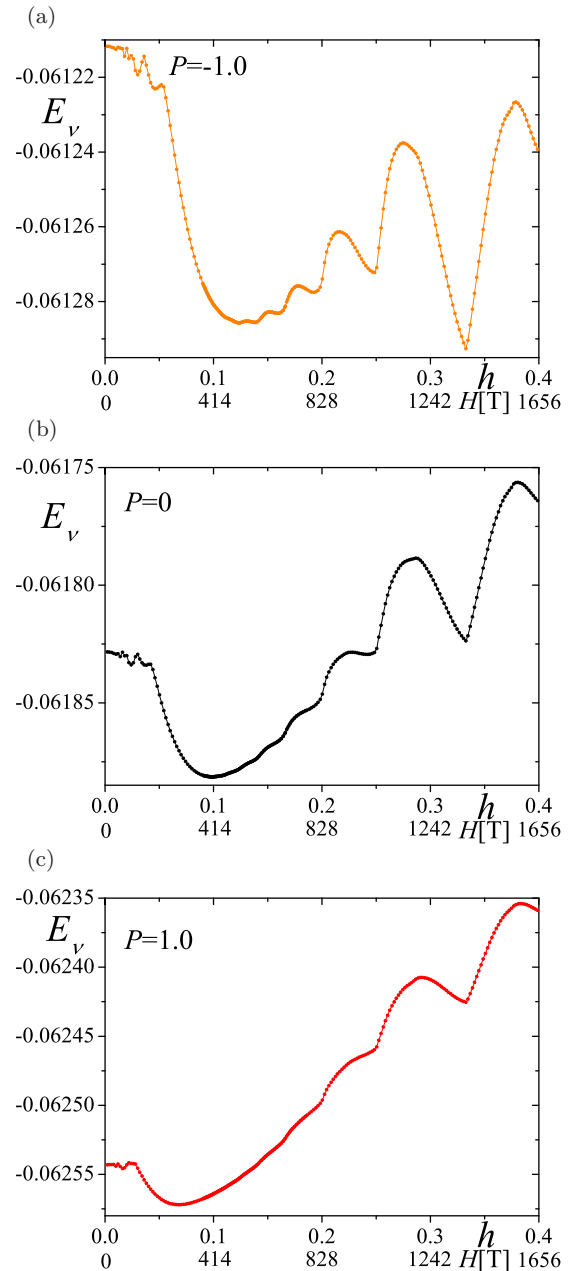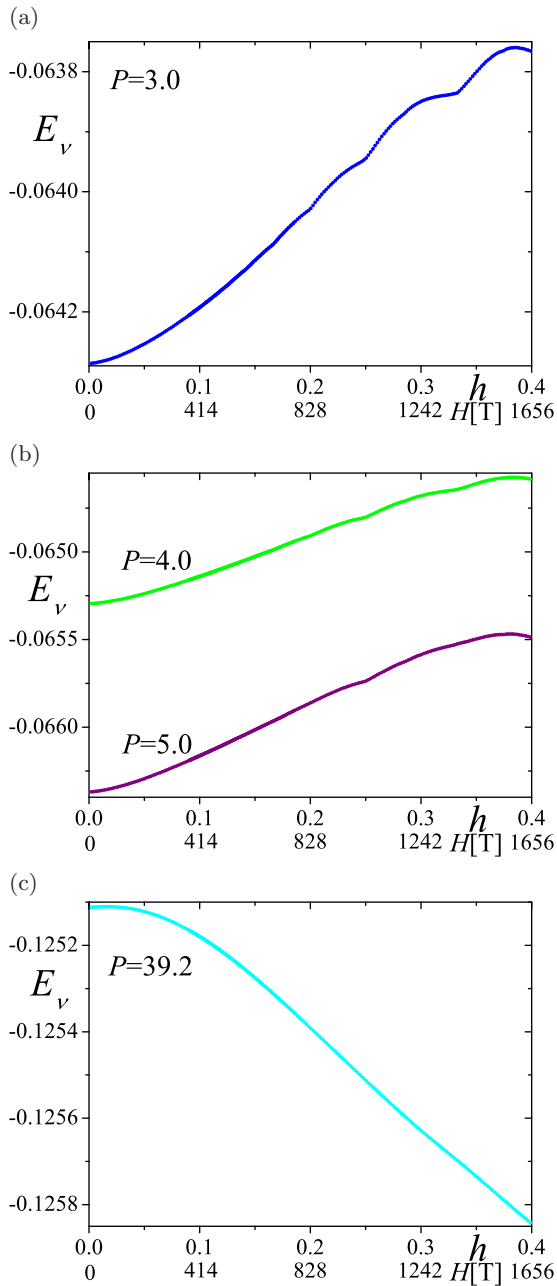
(a)

(b)

(c)

FIG. 25. Total energies as a function of h at $P = 3.0$ (a), 4.0 and 5.0 (b), and $P = 39.2$ (c). We take $h = \frac{2m}{499}$ ($m = 1,2,3,\ldots,99$), $h = \frac{2(2m-1)}{998}$ ($m = 1,2,3,\ldots,100$), and $h = \frac{32}{q}$ ($q = 173,175,\ldots,355$).

A. Semimetallic system at $P < 3.0$

At $P = -1.0$ there are an electron pocket (its area is $A_e/A_{\text{BZ}} = 0.0903$, where A_{BZ} is the area of the first Brillouin zone) and a hole pocket (A_h), as shown in Fig. 12(a). These areas are the same ($A_e = A_h$). These areas become $A_e/A_{\text{BZ}} = A_h/A_{\text{BZ}} = 0.0715$ at $P = 0$ [Fig. 12(b)]. There is a small neck in an electron pocket around $\mathbf{k} = (\pi/a,0)$ or $\mathbf{k} = (-\pi/a,0)$, as indicated by black arrows in Figs. 12(a) and 12(b). At $P \gtrsim 0.2$ an electron pocket separates around the small neck into two small electron pockets with the half area, $A_e/2$. At $P = 1.0$, $A_e/A_{\text{BZ}} = A_h/A_{\text{BZ}} = 0.0479$ and $A_e/(2A_{\text{BZ}}) = 0.0240$, as shown in Fig. 12(c).

(a)

(b)

(c)

(d)

FIG. 26. Magnetizations as a function of $1/h$ at $P = -1.0$ (a), $P = 0$ (b), $P = 1.0$ (c), and $P = 3.0$ (d), calculated by numerical differentiation of total energies in Fig. 22.

The obtained magnetizations are periodically oscillated as a function of $1/h$, as shown in Figs. 26 and 27, where main frequencies f are 0.0902 at $P = -1.0$, 0.0714 at $P = 0$, and
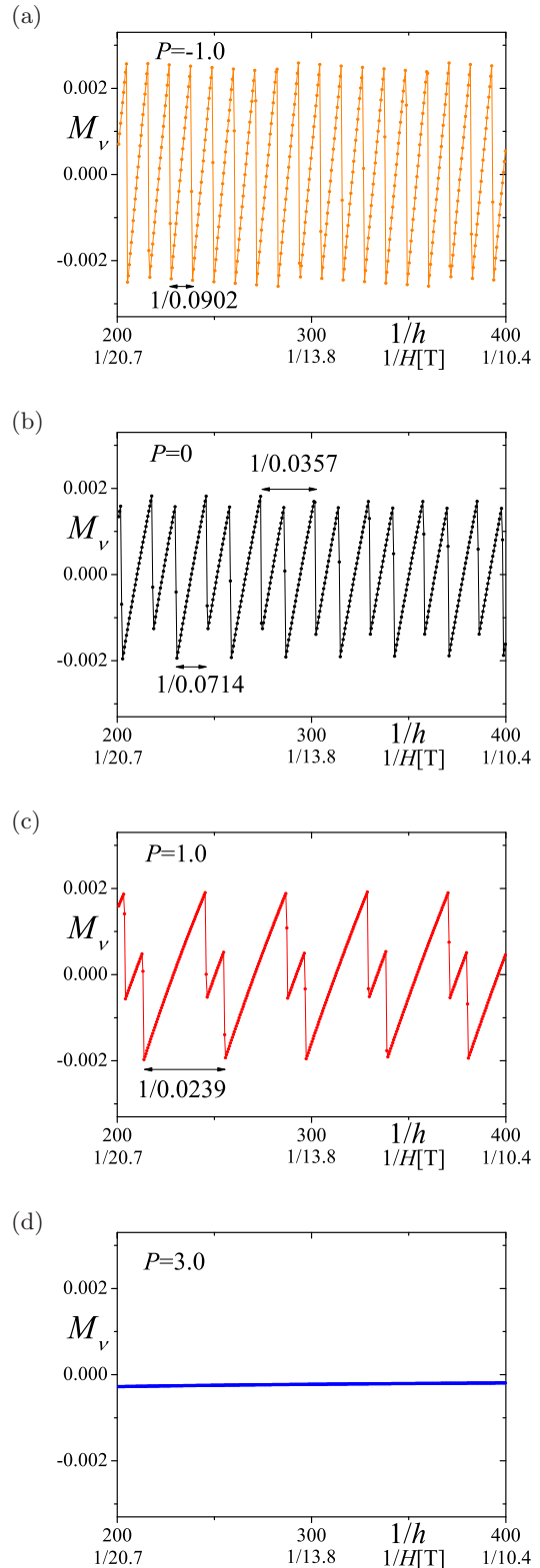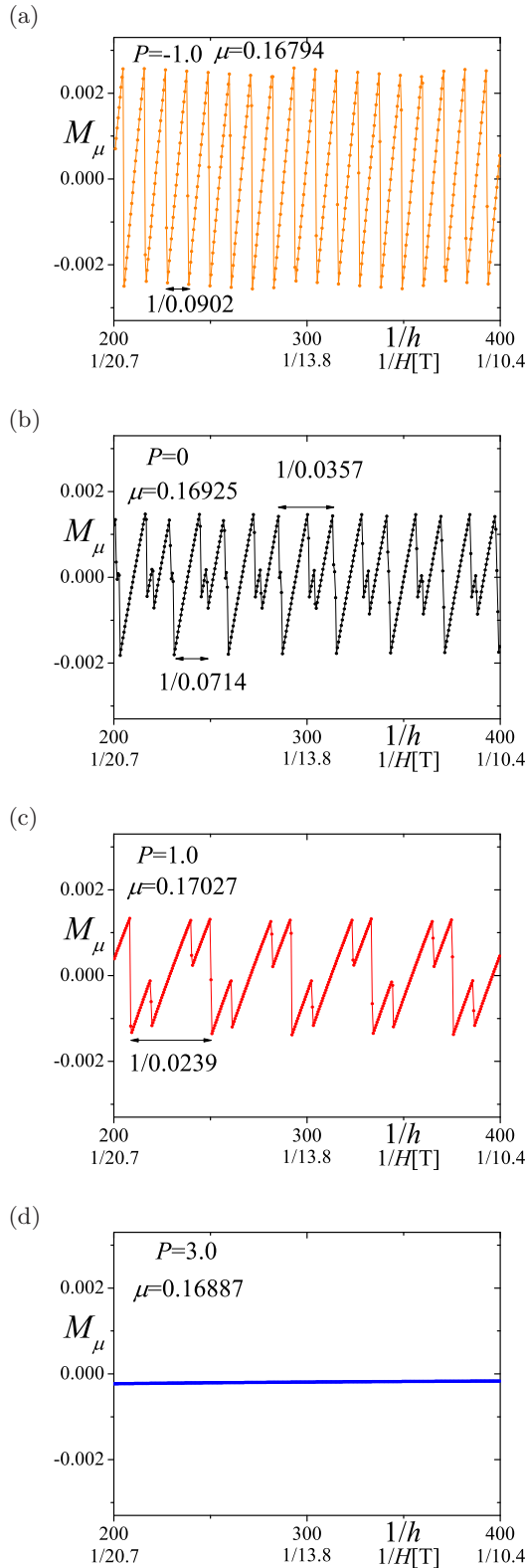
FIG. 27. Magnetizations as a function of $1/h$ at $P = -1.0$ (a), $P = 0$ (b), $P = 1.0$ (c), and $P = 3.0$ (d), calculated by the numerical differentiation of total energies in Fig. 23.

FIG. 28. Magnetizations with 3/4 filling as a function of h (a) and as a function of $1/h$ (b) at $P = -1.0, 0, 1.0, 3.0, 4.0, 5.0,$ and 39.2. The same values of $h = p/q$ as those in Figs. 24 and 25 are used.

0.0239 at $P = 1.0$. These frequencies correspond to the areas of electron and hole pockets at $h = 0$, which are considered as the dHvA oscillation. Actually, the Landau levels for an electron pocket (upward-sloping lines) and for a hole pocket (downward-sloping lines) are crossing the Fermi energy at $h = 0$ (a black dotted line), as shown in Figs. 29(a)–29(c). There is no dHvA oscillation at $P = 3.0$ in the region $1/400 \lesssim h \lesssim 1/200$, which is consistent with the fact that there are no Fermi surface at $P = 3.0$ and $h = 0$.

The Fourier transform intensities (FTIs) of M_ν and M_μ which are defined in Appendix G are plotted in Fig. 30. The FTIs of M_ν and M_μ at $P = -1.0$ are almost the same [Fig. 30(a)] because the oscillation of the Fermi energy as a function of h (a blue thin line) is small, as shown in Fig. 29(a). There are the peaks of the FTIs at $f = f_e = A_e/A_{BZ} = f_h = A_h/A_{BZ}$, $f = 2f_e = 2f_h$, $f = 3f_e = 3f_h$, etc., and the height of the lth harmonics is smaller for larger l. These are the same as that of the LK formula of a closed Fermi surface.

The FTIs of M_ν are different from those of M_μ in the cases of $P = 0$ and $P = 1.0$ [Fig. 30(b)], where the oscillations of

the Fermi energy are not small, as shown in Figs. 29(b) and 29(c).

We discuss the largest peaks at f_e and the second largest peaks at $f_e/2$ in M_ν and M_μ at $P = 0$, as shown in Fig. 30(b). The dHvA oscillation with f_e is due to the crossing of *nondegenerated* Landau levels and ε_F^0 [see Fig. 29(b)]. These Landau levels come from an electron pocket with A_e in Fig. 12(b). On the other hand, the frequency $f_e/2$ corresponds to the half area of an electron pocket [the green area in Fig. 12(b)]. The dHvA oscillation with $f_e/2$ is explained by the magnetic breakdown in the semiclassical theory (i.e., a realization of an effectively closed electron's motion by the tunneling). In our numerical study, the effect of the magnetic breakdown is taken into account naturally. Therefore, we can understand the magnetic breakdown as the separations of the Landau levels around blue circles in Fig. 29(b). When the magnetic field and the energy are lower than blue circles, the Landau levels are almost degenerated, which are due to two small electron pockets with $A_e/2$. Although these degenerated Landau levels do not cross ε_F^0 [see Fig. 29(b)], since the separations of the Landau levels (blue circles) occur below and close to ε_F^0, the dHvA oscillation with $f_e/2$ becomes finite in Fig. 30(b). At $P = -1.0$, the separations are not seen in the regions of the magnetic field and the energy [Fig. 29(a)]. As a result, there is no peak at $f_e/2$.

There are the largest peaks at $f_e/2$ in M_ν and M_μ at $P = 1.0$ [Fig. 30(c)], which is consistent with the result expected in the LK formula because of two electron pockets with $A_e/2$ [red circles in Fig. 12(c)]. Since there is a hole pocket with A_e [a blue circle in Fig. 12(c)], the dHvA oscillations with f_e and its higher harmonics are expected. In fact, ε_F^0 (a black dotted line) crosses Landau levels not only for two small electron pockets (upward-sloping lines) but also for a hole pocket (downward-sloping lines), as shown in Fig. 29(c). However, peaks at f_e and at $3f_e$ are very small. The anomalous smallness of these peaks is not expected in the LK formula.

B. Dirac fermions system at $P \geqslant 3.0$

The magnetization as a function of $1/h$ oscillates periodically with the frequency corresponding to the area of the Brillouin zone ($f = 1$) at $h \gtrsim 1/10$, corresponding to about 414 T in α-(BEDT-TTF)$_2$I$_3$, as shown in Fig. 28(b). This oscillation appears even in the case in which there is no Fermi surface ($P \geqslant 3.0$). Although the usual dHvA oscillation is caused by the crossing of the chemical potential and the Landau levels, the obtained dHvA-like oscillation is not due to the crossing. The origin of the oscillation is the Harper broadening between a blue thick line and a green thin line, as shown in Fig. 17(c).

The magnitude of this dHvA-like oscillation becomes small as $1/h$ increases. The wave form of the oscillation at $P \geqslant 3.0$ is similar to the sawtooth pattern for fixed electron number rather than the inverse sawtooth pattern in the LK formula for the fixed chemical potential (see Appendix B). The wave form at $P < 3.0$ is not sawtooth but sinusoidal-like, as shown in Fig. 28.

The dHvA-like oscillation with $f = 1$ has also been obtained on the honeycomb lattice [26]. If we use the lattice constant ($\simeq 0.246$ nm) of graphene, the oscillation appears
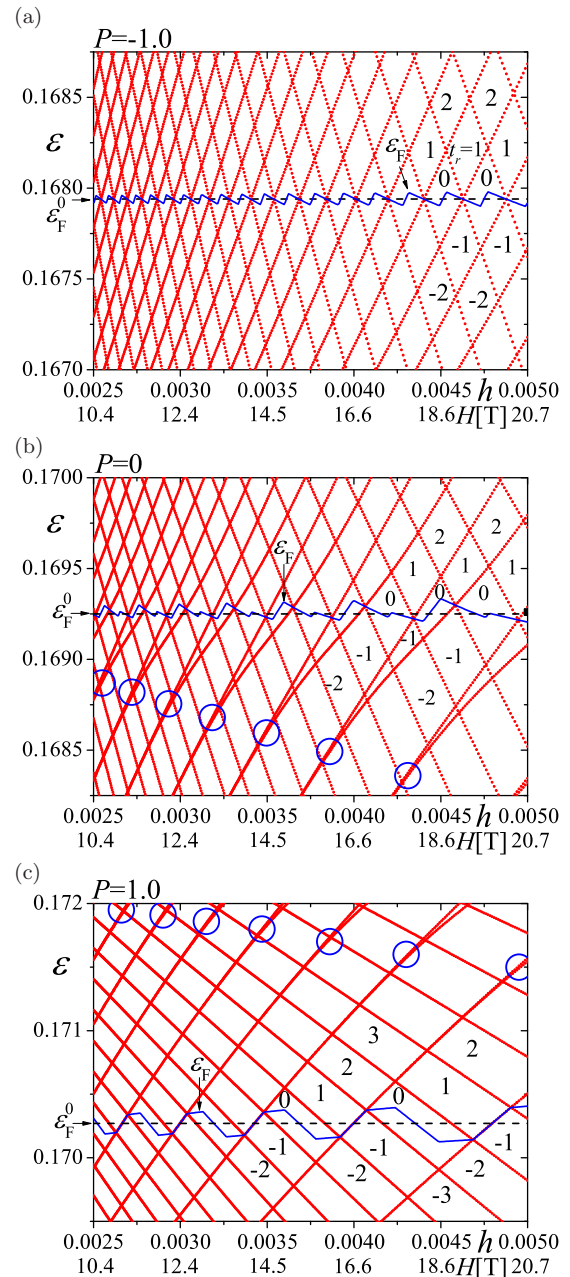
FIG. 29. Energies near the Fermi energy as a function of h at $P = -1.0$ (a), $P = 0$ (b), and $P = 1.0$ (c). We choose $p = 2$ and $400 \leqslant q \leqslant 800$ ($q = 400, 401, \ldots, 799, 800$). The energy gaps are labeled by $t_r = \pm 1$, ± 2, and ± 3 with $s_r = 3$. The Fermi energy (ε_F) for 3/4 filling at $h \neq 0$ are shown by the blue thin lines. The Fermi energies (ε_F^0) for 3/4 filling at $h = 0$ are 0.16794, 0.16925, and 0.17027 for $P = -1.0$, 0, and 1.0, respectively, which are indicated by the black broken lines.

at a very high magnetic field (~ 5000 T) [26]. Since the flux through the unit cell in α-(BEDT-TTF)$_2$I$_3$ is larger than that in graphene, it is expected to find the dHvA-like oscillation at lower magnetic field. Very recently, the dHvA-like oscillation in the system with no Fermi surface has been observed in SmB$_6$ [65] and studied theoretically in many models [66–69].

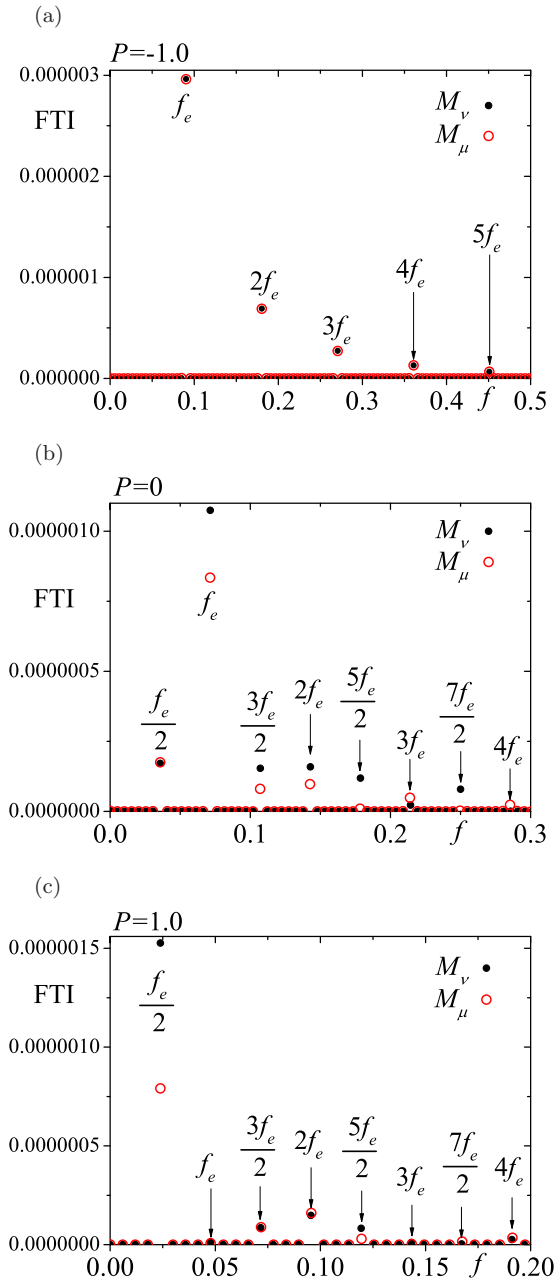FIG. 30. The FTIs of M_ν and M_μ in Fig. 26 and Fig. 27 for $P = -1.0$ (a), $P = 0$ (b), and $P = 1.0$ (c). In (a), $2L = 188.5$ and $1/h_c = 299.5$. In (b), $2L = 196$ and $1/h_c = 300.75$ for M_ν and $2L = 196.3$ and $1/h_c = 301.55$ for M_μ. In (c), $2L = 167.5$ and $1/h_c = 297.25$ for M_ν and $2L = 167.25$ and $1/h_c = 292.875$ for M_μ.

V. CONCLUSIONS

We find a "three-quarter" Dirac point in the tight-binding model of α-(BEDT-TTF)$_2$I$_3$ at $P = 2.3$ kbar, although this point is hidden by the metal-insulator transition at low temperature in the real system. At that pressure the Dirac cone is critically tilted and we have to take account of quadratic terms. Then the dispersion relation is linear in three directions and parabolic in one direction at three-quarter Dirac points.

We obtain the energy as a function of the magnetic field by taking the complex hopping integrals. We find the $H^{4/5}$

dependence due to three-quarter Dirac points at $P = 2.3$ kbar. We also obtain the H^2 dependence at the intermediate magnetic field strength at $P = 3.0$ kbar, which is caused by the laid Dirac cone.

We numerically obtain the magnetic field dependencies of the total energy and the magnetization [de Haas–van Alphen (dHvA) oscillation] in both cases of fixed electron number and fixed chemical potential. At $P = 0$ kbar we find the FTI at the frequency corresponding to half the area of an electron pocket which is not a closed orbit. This oscillation is attributed to the smooth separations of the Landau levels as a function of the magnetic field. This is a quantum mechanical picture of the magnetic breakdown. At $P = 1.0$ kbar the FTI at the frequency corresponding to the area of the hole pocket is shown to be quite small, which cannot be explained by the semiclassical LK formula.

When the system is considered to be massless Dirac fermions at $P > 3.0$ kbar, we find the unusual dHvA-like oscillation with the period corresponding to the area of the first Brillouin zone at $H \gtrsim 400$ T. This oscillation is thought to be due to the Harper broadening of the Landau levels, which is similar to the case on the honeycomb lattice [26].

Recently, the Landau levels in massless Dirac fermions have been directly observed from the scanning tunneling spectra [70]. The Landau levels for three-quarter Dirac cones and for almost laid Dirac cones are expected to be observed if the charge ordering is removed. Furthermore, the results for the usual dHvA oscillation and the unusual dHvA-like oscillation shown in this study will be observed. However, in order to suppress the charge ordering, high pressures (the uniaxial pressure of $P \gtrsim 10$ kbar [43] and the hydrostatic pressure of $P \gtrsim 11$–12 kbar [46]) are needed. Therefore, the experiments in the semimetallic state may be difficult to observe at low temperature. It will be possible to observe the obtained results, if the critically tilted Dirac cones or overtilted Dirac cones are realized in other systems such as ultracold atoms [71] and graphene under uniaxial strain [18].

APPENDIX A: SEMICLASSICAL LANDAU QUANTIZATION OF ENERGY

In the semiclassical theory, the energies of two-dimensional electrons are quantized into the Landau levels (ε_n with integer n) when the area of the closed Fermi surface in the wave-number space $A(\varepsilon_n)$ at $H = 0$ equals to the quantized value proportional to the magnetic field, i.e.,

$$A(\varepsilon_n) = (n + \gamma)\frac{2\pi e H}{\hbar c}, \qquad (A1)$$

where n is an integer, e is the electron charge, c is the speed of light, $\hbar$ is the Planck constant divided by 2π, and γ is a phase factor which can be determined from the quantum mechanical calculation ($\gamma = 1/2$ for massive free electrons and $\gamma = 0$ for massless Dirac fermions).

APPENDIX B: dHvA OSCILLATION AND LIFSHITZ AND KOSEVICH FORMULA

The magnetization in metals oscillates periodically as a function of the inverse of the magnetic field at low temperatures, which is called the dHvA oscillation [15]. The period of the dHvA oscillation is proportional to the extremal area of the closed Fermi surface in a plane perpendicular to the magnetic field in the semiclassical theory.

For the dHvA oscillation, the Lifshitz and Kosevich (LK) formula [15,34] based on the semiclassical theory [14] is derived in the case of the fixed chemical potential μ (the grand canonical ensemble). The generalized LK formula at $T = 0$ for the two-dimensional metals with no impurity is given by

$$M^{\text{LK}} = -\frac{e}{2\pi^2 c\hbar} \frac{A}{\frac{\partial A}{\partial \mu}} \sum_{l=1}^{\infty} \frac{1}{l} \sin\left[2\pi l\left(\frac{F}{H} - \gamma\right)\right], \quad \text{(B1)}$$

where its frequency (F) is given by

$$F = \frac{c\hbar A}{2\pi e}, \quad \text{(B2)}$$

where A is the area of the closed Fermi surface at $H = 0$. When we use h of Eq. (6) instead of H in Eq. (B1), we get

$$\frac{F}{H} = \frac{f}{h}, \quad \text{(B3)}$$

where

$$f = \frac{A}{A_{\text{BZ}}} \quad \text{(B4)}$$

and $A_{\text{BZ}} = 4\pi^2/(ab)$ is the area of the Brillouin zone. The amplitude of the oscillation at $T = 0$ is independent of h in the LK formula.

In the two-dimensional system with a closed Fermi surface at $h = 0$, Eq. (B1) becomes the sawtooth shape. If the electron number is fixed in that system, the chemical potential jumps from a Landau level to another Landau level as the magnetic field increases. As a result, the sawtooth pattern as a function of $1/h$ is inverted [15].

APPENDIX C: ENERGY AT $H = 0$

The Bravais lattice in our model [Fig. 1(a)] is given by

$$\mathbf{v}_1 = (a, 0) \quad \text{(C1)}$$

and

$$\mathbf{v}_2 = (0, b). \quad \text{(C2)}$$

The Hamiltonian with the hoppings between neighboring sites (t_{a1}, t_{a2}, t_{a3}, t_{b1}, t_{b2}, t_{b3}, and t_{b4}; see Fig. 1) is given by

$$\begin{aligned}
\hat{\mathcal{H}}_0 = \sum_{\mathbf{r}_j} \Big\{ &t_{a1} c_{4,\mathbf{r}_j}^\dagger c_{3,\mathbf{r}_j} + t_{a1} c_{4,\mathbf{r}_j}^\dagger c_{3,\mathbf{r}_j+\mathbf{v}_2} + t_{a2} c_{1,\mathbf{r}_j}^\dagger c_{2,\mathbf{r}_j} \\
&+ t_{a3} c_{1,\mathbf{r}_j}^\dagger c_{2,\mathbf{r}_j-\mathbf{v}_2} + t_{b1} c_{1,\mathbf{r}_j}^\dagger c_{4,\mathbf{r}_j} + t_{b1} c_{2,\mathbf{r}_j}^\dagger c_{4,\mathbf{r}_j-\mathbf{v}_1} \\
&+ t_{b2} c_{1,\mathbf{r}_j}^\dagger c_{3,\mathbf{r}_j} + t_{b2} c_{2,\mathbf{r}_j}^\dagger c_{3,\mathbf{r}_j-\mathbf{v}_1+\mathbf{v}_2} + t_{b3} c_{1,\mathbf{r}_j}^\dagger c_{3,\mathbf{r}_j-\mathbf{v}_1} \\
&+ t_{b3} c_{2,\mathbf{r}_j}^\dagger c_{3,\mathbf{r}_j+\mathbf{v}_2} + t_{b4} c_{1,\mathbf{r}_j}^\dagger c_{4,\mathbf{r}_j-\mathbf{v}_1} + t_{b4} c_{2,\mathbf{r}_j}^\dagger c_{4,\mathbf{r}_j} + \text{H.c.} \Big\},
\end{aligned} \quad \text{(C3)}$$

where $c_{1,\mathbf{r}_j}^\dagger$, $c_{2,\mathbf{r}_j}^\dagger$, $c_{3,\mathbf{r}_j}^\dagger$, and $c_{4,\mathbf{r}_j}^\dagger$ ($c_{1,\mathbf{r}_j}$, $c_{2,\mathbf{r}_j}$, $c_{3,\mathbf{r}_j}$, and $c_{4,\mathbf{r}_j}$) are creation (annihilation) operators for 1, 2, 3, and 4 sites in the jth unit cell, respectively. By using the following Fourier transform,

$$c_{1,\mathbf{r}_j} = \sum_{\mathbf{k}} e^{i\mathbf{k}\cdot\mathbf{r}_j} c_{1,\mathbf{k}}, \quad \text{(C4)}$$

$$c_{2,\mathbf{r}_j} = \sum_{\mathbf{k}} e^{i\mathbf{k}\cdot(\mathbf{r}_j+\mathbf{v}_2/2)} c_{2,\mathbf{k}}, \quad \text{(C5)}$$

$$c_{3,\mathbf{r}_j} = \sum_{\mathbf{k}} e^{i\mathbf{k}\cdot(\mathbf{r}_j+\mathbf{v}_1/2-\mathbf{v}_2/4)} c_{3,\mathbf{k}}, \quad \text{(C6)}$$

$$c_{4,\mathbf{r}_j} = \sum_{\mathbf{k}} e^{i\mathbf{k}\cdot(\mathbf{r}_j+\mathbf{v}_1/2+\mathbf{v}_2/4)} c_{4,\mathbf{k}}, \quad \text{(C7)}$$

we obtain the Hamiltonian as

$$\hat{\mathcal{H}}_0 = \sum_{\mathbf{k}} C_{\mathbf{k}}^\dagger \hat{\varepsilon}_{\mathbf{k}} C_{\mathbf{k}}, \quad \text{(C8)}$$

where

$$C_{\mathbf{k}}^\dagger = (c_{1,\mathbf{k}}^\dagger, c_{2,\mathbf{k}}^\dagger, c_{3,\mathbf{k}}^\dagger, c_{4,\mathbf{k}}^\dagger), \quad \text{(C9)}$$

$$C_{\mathbf{k}} = \begin{pmatrix} c_{1,\mathbf{k}} \\ c_{2,\mathbf{k}} \\ c_{3,\mathbf{k}} \\ c_{4,\mathbf{k}} \end{pmatrix}, \quad \text{(C10)}$$

and $\hat{\varepsilon}_{\mathbf{k}}$ is a 4×4 matrix as follows:

$$\hat{\varepsilon}_{\mathbf{k}} = \begin{pmatrix} 0 & A_2 & B_2 & B_1 \\ A_2^* & 0 & B_2^* & B_1^* \\ B_2^* & B_2 & 0 & A_1 \\ B_1^* & B_1 & A_1 & 0 \end{pmatrix}, \quad \text{(C11)}$$

with

$$A_1 = 2t_{a1} \cos\frac{k_y}{2}, \quad \text{(C12)}$$

$$A_2 = t_{a2} e^{i\frac{1}{2}k_y} + t_{a3} e^{-i\frac{1}{2}k_y}, \quad \text{(C13)}$$

$$B_1 = t_{b1} e^{i(\frac{1}{2}k_x+\frac{1}{4}k_y)} + t_{b4} e^{i(-\frac{1}{2}k_x+\frac{1}{4}k_y)}, \quad \text{(C14)}$$

$$B_2 = t_{b2} e^{i(\frac{1}{2}k_x-\frac{1}{4}k_y)} + t_{b3} e^{i(-\frac{1}{2}k_x-\frac{1}{4}k_y)}. \quad \text{(C15)}$$

If $t_{a1} = t_{a2} = t_{a3} = 0$ (i.e., $A_1 = A_2 = 0$), the eigenvalues of the matrix in Eq. (C11) are obtained by Mori [48] as

$$\varepsilon_{\mathbf{k}}^0 = \pm\sqrt{|B_1|^2 + |B_2|^2 \pm \sqrt{(B_1^2 + B_2^2)(B_1^{*2} + B_2^{*2})}}. \quad \text{(C16)}$$

When A_1 and A_2 are not zero, the eigenvalues are not simple, although the analytical solutions can be obtained because of the quartic equation. We studied the energy in cases of both the bulk state and the edge state [72].

APPENDIX D: ENERGY AT $H \neq 0$

The Hamiltonian in the two-dimensional tight-binding model in the magnetic field becomes

$$\hat{\mathcal{H}} = \sum_{i,j} t_{ij} e^{i2\pi\phi_{ij}} c_i^\dagger c_j, \quad \text{(D1)}$$

where the phase factor (ϕ_{ij}) is given by

$$\phi_{ij} = \frac{e}{ch} \int_j^i \mathbf{A} \cdot d\mathbf{l}. \tag{D2}$$

In this study, we treat the magnetic field applied perpendicular to the x-y plane by taking the ordinary Landau gauge,

$$\mathbf{A} = (Hy, 0, 0). \tag{D3}$$

The flux through the unit cell is

$$\Phi = abH. \tag{D4}$$

When the magnetic field is commensurate with the lattice period, i.e.,

$$\frac{\Phi}{\phi_0} = \frac{p}{q}, \tag{D5}$$

where p and q are integers, the magnetic unit cell is $a \times (qb)$, if p is an even integer. Since there are two sites with half of the lattice constant in the y direction in the unit cell, we have to take the magnetic unit cell of $a \times (2qb)$, if we take the ordinary Landau gauge and p is an odd integer. We can take a more suitable gauge (periodic Landau gauge) [73], which is a powerful tool for the system with a large unit cell such as the moiré pattern in the twisted bilayer graphene. However, we take even integers for p by using the ordinary Landau gauge in this paper, since it is possible to investigate magnetic field dependencies of energies only by taking even integers for p.

The Hamiltonian in the momentum space becomes

$$\hat{\mathcal{H}} = \sum_{\mathbf{k}} \tilde{C}_{\mathbf{k}}^\dagger \tilde{\varepsilon}_{\mathbf{k}} \tilde{C}_{\mathbf{k}}, \tag{D6}$$

where the summation over $\mathbf{k}$ is taken in the magnetic Brillouin zone,

$$-\frac{\pi}{a} \leqslant k_x < \frac{\pi}{a}, \tag{D7}$$

$$-\frac{\pi}{qb} \leqslant k_y < \frac{\pi}{qb}. \tag{D8}$$

In Eq. (D6), the creation and annihilation operators have $4q$ components,

$$\tilde{C}_{\mathbf{k}}^\dagger = (c_{1,\mathbf{k}}^{(0)\dagger}, c_{2,\mathbf{k}}^{(0)\dagger}, c_{3,\mathbf{k}}^{(0)\dagger}, c_{4,\mathbf{k}}^{(0)\dagger}, \ldots, c_{3,\mathbf{k}}^{(q-1)\dagger}, c_{4,\mathbf{k}}^{(q-1)\dagger}), \tag{D9}$$

$$\tilde{C}_{\mathbf{k}} = \begin{pmatrix} c_{1,\mathbf{k}}^{(0)} \\ c_{2,\mathbf{k}}^{(0)} \\ c_{3,\mathbf{k}}^{(0)} \\ c_{4,\mathbf{k}}^{(0)} \\ \cdot \\ \cdot \\ \cdot \\ c_{3,\mathbf{k}}^{(q-1)} \\ c_{4,\mathbf{k}}^{(q-1)} \end{pmatrix} \tag{D10}$$

and $\tilde{\varepsilon}_{\mathbf{k}}$ is the $4q \times 4q$ matrix which is given by

$$\tilde{\varepsilon}_{\mathbf{k}} = \begin{pmatrix} D_{\mathbf{k}}^{(0)} & F_{\mathbf{k}}^{(1)} & 0 & \cdots & & 0 & F_{\mathbf{k}}^{(0)\dagger} \\ F_{\mathbf{k}}^{(1)\dagger} & D_{\mathbf{k}}^{(1)} & F_{\mathbf{k}}^{(2)} & \ddots & & \ddots & 0 \\ 0 & F_{\mathbf{k}}^{(2)\dagger} & D_{\mathbf{k}}^{(2)} & F_{\mathbf{k}}^{(3)} & & \ddots & \vdots \\ \vdots & \ddots & \ddots & \ddots & & \ddots & 0 \\ 0 & \ddots & & \ddots & F_{\mathbf{k}}^{(q-2)\dagger} & D_{\mathbf{k}}^{(q-2)} & F_{\mathbf{k}}^{(q-1)} \\ F_{\mathbf{k}}^{(0)} & 0 & & \cdots & 0 & F_{\mathbf{k}}^{(q-1)\dagger} & D_{\mathbf{k}}^{(q-1)} \end{pmatrix}, \tag{D11}$$

where

$$D_{\mathbf{k}}^{(n)} = \begin{pmatrix} 0 & \epsilon_{\mathbf{k}12}^{(n)} & \epsilon_{\mathbf{k}13}^{(n)} & \epsilon_{\mathbf{k}14}^{(n)} \\ \epsilon_{\mathbf{k}12}^{(n)*} & 0 & 0 & \epsilon_{\mathbf{k}24}^{(n)} \\ \epsilon_{\mathbf{k}13}^{(n)*} & 0 & 0 & \epsilon_{\mathbf{k}34}^{(n)} \\ \epsilon_{\mathbf{k}14}^{(n)*} & \epsilon_{\mathbf{k}24}^{(n)*} & \epsilon_{\mathbf{k}34}^{(n)*} & 0 \end{pmatrix}, \tag{D12}$$

$$F_{\mathbf{k}}^{(n)} = \begin{pmatrix} 0 & 0 & 0 & 0 \\ \epsilon_{\mathbf{k}21}^{\prime(n)} & 0 & \epsilon_{\mathbf{k}23}^{\prime(n)} & 0 \\ 0 & 0 & 0 & 0 \\ 0 & 0 & \epsilon_{\mathbf{k}43}^{\prime(n)} & 0 \end{pmatrix}, \tag{D13}$$

and

$$F_{\mathbf{k}}^{(n)\dagger} = \begin{pmatrix} 0 & \epsilon_{\mathbf{k}21}^{\prime(n)*} & 0 & 0 \\ 0 & 0 & 0 & 0 \\ 0 & \epsilon_{\mathbf{k}23}^{\prime(n)*} & 0 & \epsilon_{\mathbf{k}43}^{\prime(n)*} \\ 0 & 0 & 0 & 0 \end{pmatrix}. \tag{D14}$$

The matrix elements, $\varepsilon_{\mathbf{k}\alpha\beta}^{(n)}$, are the hoppings from the β site (j) in the nth unit cell to the α site (i) in the nth unit cell in the magnetic field [$nb \leqslant y_j < (n+1)b$ and $nb \leqslant y_i < (n+1)b$] given by

$$\epsilon_{\mathbf{k}12}^{(n)} = t_{a2} e^{i\frac{1}{2}bk_y}, \tag{D15}$$

$$\epsilon_{\mathbf{k}13}^{(n)} = t_{b2} \exp\left[i\left(\frac{1}{2}ak_x - \frac{1}{4}bk_y + 2\pi\phi_{b2,13}^{(n)}\right)\right]$$
$$+ t_{b3} \exp\left[i\left(-\frac{1}{2}ak_x - \frac{1}{4}bk_y + 2\pi\phi_{b3,13}^{(n)}\right)\right], \tag{D16}$$

$$\epsilon_{\mathbf{k}14}^{(n)} = t_{b1} \exp\left[i\left(\frac{1}{2}ak_x + \frac{1}{4}bk_y + 2\pi\phi_{b1,14}^{(n)}\right)\right]$$
$$+ t_{b4} \exp\left[i\left(-\frac{1}{2}ak_x + \frac{1}{4}bk_y + 2\pi\phi_{b4,14}^{(n)}\right)\right], \tag{D17}$$

$$\epsilon_{\mathbf{k}24}^{(n)} = t_{b1} \exp\left[i\left(-\frac{1}{2}ak_x - \frac{1}{4}bk_y + 2\pi\phi_{b1,24}^{(n)}\right)\right]$$
$$+ t_{b4} \exp\left[i\left(\frac{1}{2}ak_x - \frac{1}{4}bk_y + 2\pi\phi_{b4,24}^{(n)}\right)\right], \tag{D18}$$

$$\epsilon_{\mathbf{k}34}^{(n)} = t_{a1} e^{i\frac{1}{2}bk_y}, \tag{D19}$$

where

$$\phi_{b2,13}^{(n)} = \frac{\Phi}{\phi_0}\left(\frac{n}{2} - \frac{1}{16}\right), \tag{D20}$$

$$\phi_{b3,13}^{(n)} = -\frac{\Phi}{\phi_0}\left(\frac{n}{2} - \frac{1}{16}\right), \tag{D21}$$

$$\phi_{b1,14}^{(n)} = \frac{\Phi}{\phi_0}\left(\frac{n}{2} + \frac{1}{16}\right), \tag{D22}$$

$$\phi_{b4,14}^{(n)} = -\frac{\Phi}{\phi_0}\left(\frac{n}{2} + \frac{1}{16}\right), \tag{D23}$$

$$\phi_{b1,24}^{(n)} = -\frac{\Phi}{\phi_0}\left(\frac{n}{2} + \frac{3}{16}\right), \tag{D24}$$

$$\phi_{b4,24}^{(n)} = \frac{\Phi}{\phi_0}\left(\frac{n}{2} + \frac{3}{16}\right). \tag{D25}$$

The matrix elements, $\epsilon_{\mathbf{k}\alpha\beta}'^{(n)}$, are the hoppings from the β site (j) in the $(n+1)$th unit cell to the α site (i) in the nth unit cell in the magnetic field $[(n+1)b \leqslant y_j < (n+2)b$ and $nb \leqslant y_i < (n+1)b]$ given by

$$\epsilon_{\mathbf{k}21}'^{(n)} = t_{a3}e^{i\frac{1}{2}bk_y}, \tag{D26}$$

$$\epsilon_{\mathbf{k}23}'^{(n)} = t_{b2}\exp\left[i\left(-\frac{1}{2}ak_x + \frac{1}{4}bk_y + 2\pi\phi_{b2,23}'^{(n)}\right)\right]$$
$$+ t_{b3}\exp\left[i\left(\frac{1}{2}ak_x + \frac{1}{4}bk_y + 2\pi\phi_{b3,23}'^{(n)}\right)\right], \tag{D27}$$

$$\epsilon_{\mathbf{k}43}'^{(n)} = t_{a1}e^{i\frac{1}{2}bk_y}, \tag{D28}$$

where

$$\phi_{b2,23}'^{(n)} = -\frac{\Phi}{\phi_0}\left(\frac{n}{2} - \frac{3}{16}\right), \tag{D29}$$

$$\phi_{b3,23}'^{(n)} = \frac{\Phi}{\phi_0}\left(\frac{n}{2} - \frac{3}{16}\right). \tag{D30}$$

APPENDIX E: DERIVATION OF EQ. (5)

The critical pressure, $P_c = 3.0$, is defined by the pressure at which the global maximum energy of the third band, ε_{3t}^0, becomes the same as the energy at the Dirac points ε_D^0. At $2.3 < P \lesssim P_c$, ε_{3t}^0 and ε_D^0 depend on pressure as

$$\varepsilon_{3t}^0 = a_{3t}(P_c - P) + \varepsilon_D^{00}, \tag{E1}$$

$$\varepsilon_D^0 = -a_D(P_c - P) + \varepsilon_D^{00}, \tag{E2}$$

respectively, where a_{3t} and a_D are pressure-independent constant and ε_D^{00} is the energy at the Dirac points at $P = P_c$. The densities of states at the third band and the fourth band are given by

$$D_3(\varepsilon^0) = d_3\theta(\varepsilon_{3t}^0 - \varepsilon^0), \tag{E3}$$

$$D_4(\varepsilon^0) = c_D(\varepsilon^0 - \varepsilon_D^0), \tag{E4}$$
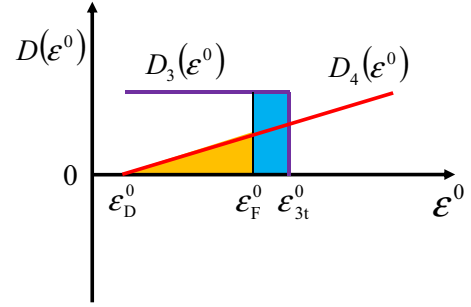

FIG. 31. A schematic plot of the density of states at $P < P_c$.

where d_3 and c_D are constants and $\theta(\varepsilon_{3t}^0 - \varepsilon^0)$ is the step function, as shown in Fig. 31.

The Fermi energy ε_F^0 at $P \lesssim P_c$ is obtained by the condition that the area of a hole pocket equals that of an electron pocket, i.e.,

$$\int_{\varepsilon_F^0}^{\varepsilon_{3t}^0} D_3(\varepsilon^0)d\varepsilon^0 = \int_{\varepsilon_D^0}^{\varepsilon_F^0} D_4(\varepsilon^0)d\varepsilon^0. \tag{E5}$$

By putting Eqs. (E3) and (E4) into Eq. (E5), we obtain

$$d_3\left(\varepsilon_{3t}^0 - \varepsilon_F^0\right) = \tfrac{1}{2}c_D\left(\varepsilon_F^0 - \varepsilon_D^0\right)^2. \tag{E6}$$

We study the cases of

$$P_c - P \ll P_c \tag{E7}$$

and

$$\varepsilon_D^0 < \varepsilon_F^0 < \varepsilon_{3t}^0. \tag{E8}$$

Since

$$\varepsilon_{3t}^0 - \varepsilon_D^0 = (a_{3t} + a_D)(P_c - P) \tag{E9}$$

goes to zero when $P_c - P \to 0$, we obtain that both $\varepsilon_{3t}^0 - \varepsilon_F^0$ and $\varepsilon_F^0 - \varepsilon_{3t}^0$ go to zero when $P_c - P \to 0$. By using

$$\varepsilon_F^0 - \varepsilon_D^0 = (a_{3t} + a_D)(P_c - P) - \left(\varepsilon_{3t}^0 - \varepsilon_F^0\right) \tag{E10}$$

and Eq. (E6), we obtain

$$\varepsilon_F^0 - \varepsilon_D^0 \simeq (a_{3t} + a_D)(P_c - P) + O((P_c - P)^2), \tag{E11}$$

$$\varepsilon_{3t}^0 - \varepsilon_F^0 \simeq \frac{c_D}{2d_3}(a_{3t} + a_D)^2(P_c - P)^2. \tag{E12}$$

APPENDIX F: THREE-QUARTER DIRAC POINT AND DERIVATION OF EQ. (12)

In this appendix we derive the area as a function of energy around the three-quarter Dirac point, Eq. (12). The minimal Weyl Hamiltonian studied by Goerbig, Fuchs, and Montambaux [18] is given by

$$\mathcal{H}_{\text{Weyl}}^0 = \mathbf{w}_0 \cdot \mathbf{q}\sigma^0 + w_x q_x \sigma^x + w_y q_y \sigma^y, \tag{F1}$$

where σ^0 is a 2×2 unit matrix, σ^x and σ^y are the Pauli matrices, and $\mathbf{w}_0 = (w_{0x}, w_{0y})$, w_x, and w_y are constants. The

energy dispersion is given by

$$\varepsilon^0_\pm(\mathbf{q}) = \mathbf{w}_0 \cdot \mathbf{q} \pm \sqrt{w_x^2 q_x^2 + w_y^2 q_y^2}. \tag{F2}$$

The anisotropy and the tilting of the Dirac cone are described by w_x and w_y and by w_{0x} and w_{0y}, respectively. For simplicity we take $w_x > 0$ and $w_y > 0$. The energy of the tilted Dirac cone has also been studied in the linearized form in the context of type II Weyl semimetals [74].

When we take

$$w_{0y} = 0, \tag{F3}$$

$$w_{0x} = -w_x < 0, \tag{F4}$$

the Dirac cone is critically tilted. In this case, we have to introduce quadratic terms along the q_x axis as

$$\mathcal{H}^0_{\text{tqD}} = \left(-w_x q_x + \alpha'_2 q_x^2\right)\sigma^0 + \left(w_x q_x + \alpha''_2 q_x^2\right)\sigma^x + w_y q_y \sigma^y \tag{F5}$$

and obtain

$$\varepsilon^0_{\text{tqD}\pm}(\mathbf{q}) = -w_x q_x + \alpha'_2 q_x^2$$
$$\pm \sqrt{\left(w_x q_x + \alpha''_2 q_x^2\right)^2 + (w_y q_y)^2}. \tag{F6}$$

The energy dispersions of the upper band $[\varepsilon^0_{\text{tqD}+}(\mathbf{q})]$ and the lower band $[\varepsilon^0_{\text{tqD}-}(\mathbf{q})]$ near $\mathbf{q} = (0,0)$ are given by

$$\varepsilon^0_{\text{tqD}+}(q_x, q_y = 0) = \begin{cases} \alpha_2 q_x^2, & \text{if } q_x > 0, \\ 2w_x|q_x| + \tilde{\alpha}_2 q_x^2, & \text{if } q_x < 0, \end{cases} \tag{F7}$$

$$\varepsilon^0_{\text{tqD}+}(q_x = 0, q_y) = w_y|q_y|, \tag{F8}$$

$$\varepsilon^0_{\text{tqD}-}(q_x, q_y = 0) = \begin{cases} -2w_x q_x + \tilde{\alpha}_2 q_x^2, & \text{if } q_x > 0, \\ \alpha_2 q_x^2, & \text{if } q_x < 0, \end{cases} \tag{F9}$$

$$\varepsilon^0_{\text{tqD}-}(q_x = 0, q_y) = -w_y|q_y|, \tag{F10}$$

where

$$\alpha_2 = \alpha'_2 + \alpha''_2 \tag{F11}$$

and

$$\tilde{\alpha}_2 = \alpha'_2 - \alpha''_2. \tag{F12}$$

We take $\alpha_2 > 0$ for simplicity. Then $\mathbf{q} = 0$ is a local minimum of $\varepsilon_{\text{tqD}+}(\mathbf{q})$. From Eqs. (F7) and (F9), it is found that the dispersions of $\varepsilon_{\text{tqD}+}(\mathbf{q})$ and $\varepsilon_{\text{tqD}-}(\mathbf{q})$ near $\mathbf{q} = 0$ are linear in three directions and quadratic in one direction. This can reproduce the dispersion near the Fermi energy in α-(BEDT-TTF)$_2$I$_3$ at $P = 2.3$. Therefore, we consider Eq. (F5) at $\alpha_2 > 0$ as a model of the three-quarter Dirac cone. The point of $\mathbf{q} = 0$ is a three-quarter Dirac point.

Next, we calculate the area of the closed constant energy line of the fourth band by using Eq. (F6). We set $\varepsilon_{\text{tqD}+}(\mathbf{q}) = \varepsilon$ and $\varepsilon > 0$. The constant energy line is described by

$$w_y q_{y\text{F}}(q_x)$$

$$= \pm\sqrt{\left(\varepsilon + w_x q_x - \alpha'_2 q_x^2\right)^2 - \left(w_x q_x + \alpha''_2 q_x^2\right)^2}$$
$$= \sqrt{\alpha_2 \tilde{\alpha}_2 (q_x - q_{x0})(q_x - q_{x1})(q_x - q_{x2})(q_x - q_{x3})}, \tag{F13}$$

where

$$q_{x0} = -\sqrt{\frac{\varepsilon}{\alpha_2}}, \tag{F14}$$

$$q_{x1} = \frac{w_x - \sqrt{w_x^2 + \tilde{\alpha}_2 \varepsilon}}{\tilde{\alpha}_2}$$
$$\simeq -\frac{\varepsilon}{2w_x}, \tag{F15}$$

$$q_{x2} = \sqrt{\frac{\varepsilon}{\alpha_2}}, \tag{F16}$$

$$q_{x3} = \frac{w_x + \sqrt{w_x^2 + \tilde{\alpha}_2 \varepsilon}}{\tilde{\alpha}_2}$$
$$\simeq \frac{2w_x}{\tilde{\alpha}_2}. \tag{F17}$$

Note

$$q_{x0} \ll q_{x1} < 0 < q_{x2} \ll |q_{x3}|. \tag{F18}$$

The area is calculated by

$$A(\varepsilon) = 2\int_{q_{x1}}^{q_{x2}} q_{y\text{F}}(q_x)dq_x. \tag{F19}$$

By taking an approximation that an electron pocket is elliptic, we obtain from Eq. (F13) and Eq. (F19)

$$A(\varepsilon) \simeq \frac{2}{w_y}\int_{q_{x1}}^{q_{x2}} \sqrt{\alpha_2 \tilde{\alpha}_2 q_{x0} q_{x3}(q_x - q_{x1})(q_x - q_{x2})}dq_x$$

$$\simeq \frac{2}{w_y}\sqrt{\alpha_2 \tilde{\alpha}_2 \sqrt{\frac{\varepsilon}{\alpha_2}}\frac{2w_x}{\tilde{\alpha}_2}}\frac{\pi}{8}\left(\sqrt{\frac{\epsilon}{\alpha_2}} + \frac{\epsilon}{2w_x}\right)^2$$

$$\simeq \frac{\sqrt{2w_x}\pi}{4w_y}\alpha_2^{-\frac{3}{4}}\varepsilon^{\frac{5}{4}}. \tag{F20}$$

APPENDIX G: FOURIER TRANSFORM INTENSITIES

In order to analyze the oscillations in the magnetization, we calculate the Fourier transform intensities numerically as follows. By choosing the center h_c and a finite range $2L$, we calculate

$$\text{FTI}^{(1/h)}\left(f, \frac{1}{h_c}, L\right) = \left|\frac{1}{2L}\int_{\frac{1}{h_c}-L}^{\frac{1}{h_c}+L} M(h)e^{2\pi i \frac{f}{h}}d\left(\frac{1}{h}\right)\right|^2, \tag{G1}$$

where we take $f = j/(2L)$ with integer j ($j = 512$ is used in this study).

[1] For a review, see T. Ishiguro, K. Yamaji, and G. Saito, *Organic Superconductors*, 2nd ed. (Springer-Verlag, Berlin, 1998).

[2] For a recent review, see A. G. Lebed, editor, *The Physics of Organic Superconductors and Conductors* (Springer, Berlin, 2008).

[3] S. Katayama, A. Kobayashi, and Y. Suzumura, J. Phys. Soc. Jpn. **75**, 054705 (2006).

[4] A. Kobayashi, S. Katayama, Y. Suzumura, and H. Fukuyama, J. Phys. Soc. Jpn. **76**, 034711 (2007).

[5] K. Kajita, Y. Nishio, N. Tajima, Y. Suzumura, and A. Kobayashi, J. Phys. Soc. Jpn. **83**, 072002 (2014).

[6] M. Hirata, K. Ishikawa, K. Miyagawa, K. Kanoda, and M. Tamura, Phys. Rev. B **84**, 125133 (2011).

[7] T. Konoike. K. Uchida and T. Osada, J. Phys. Soc. Jpn. **81**, 043601 (2012).

[8] T. Osada, J. Phys. Soc. Jpn. **77**, 084711 (2008).

[9] Y. Hasegawa, R. Konno, H. Nakano, and M. Kohmoto, Phys. Rev. B **74**, 033413 (2006).

[10] P. Dietl, F. Piechon, and G. Montambaux, Phys. Rev. Lett. **100**, 236405 (2008).

[11] S. Banerjee, R. R. P. Singh, V. Pardo, and W. E. Pickett, Phys. Rev. Lett. **103**, 016402 (2009).

[12] G. Montambaux, F. Piechon, J. N. Fuchs, and M. O. Goerbig, Phys. Rev. B **80**, 153412 (2009).

[13] Y. Suzumura, T. Morinari, and F. Piechon, J. Phys. Soc. Jpn. **82**, 023708 (2013).

[14] L. Onsager, Philos. Mag. **43**, 1006 (1952).

[15] D. Schoenberg, *Magnetic Oscillation in Metals* (Cambridge University Press, Cambridge, 1984).

[16] J. W. McClure, Phys. Rev. **104**, 666 (1956).

[17] K. S. Novoselov, A. K. Geim, S. V. Morozov, D. Jiang, M. I. Katsnelson, I. V. Grigorieva, S. V. Dubonos, and A. A. Firsov, Nature (London) **438**, 197 (2005).

[18] M. O. Goerbig, J. N. Fuchs, G. Montambaux, and F. Piechon, Phys. Rev. B **78**, 045415 (2008).

[19] T. Morinari, T. Himura, and T. Tohyama, J. Phys. Soc. Jpn. **78**, 023704 (2009).

[20] P. G. Harper, Proc. Phys. Soc., London, Sect. A **68**, 874 (1955).

[21] D. R. Hofstadter, Phys. Rev. B **14**, 2239 (1976).

[22] Y. Hasegawa, P. Lederer, T. M. Rice, and P. B. Wiegmann, Phys. Rev. Lett. **63**, 907 (1989).

[23] Y. Hasegawa, Y. Hatsugai, M. Kohmoto, and G. Montambaux, Phys. Rev. B **41**, 9174 (1990).

[24] R. Rammal, J. Phys. (Paris) **46**, 1345 (1985).

[25] Y. Hasegawa and M. Kohmoto, Phys. Rev. B **74**, 155415 (2006).

[26] K. Kishigi and Y. Hasegawa, Phys. Rev. B **90**, 085427 (2014).

[27] J. P. Pouget, R. Moret, R. Comes, and K. Bechgaard, J. Phys. (Paris) Lett. **42**, 543 (1981).

[28] D. Vignolles, A. Audouard, M. Nardone, L. Brossard, S. Bouguessa, and J. M. Fabre, Phys. Rev. B **71**, 020404 (2005).

[29] W. Kang and Ok-Hee Chung, Phys. Rev. B **79**, 045115 (2009).

[30] J. Y. Fortin and A. Audouard, Phys. Rev. B **77**, 134440 (2008).

[31] J. Y. Fortin and A. Audouard, Phys. Rev. B **80**, 214407 (2009).

[32] A. B. Pippard, Proc. R. Soc. London, Ser. A **270**, 1 (1962).

[33] L. M. Falicov and H. Stachoviak, Phys. Rev. **147**, 505 (1966).

[34] I. M. Lifshitz and A. M. Kosevich, Sov. Phys. JETP **2**, 636 (1956).

[35] I. A. Luk'yanchuk and Y. Kopelevich, Phys. Rev. Lett. **93**, 166402 (2004).

[36] I. A. Luk'yanchuk, Low Temp. Phys. **37**, 45 (2011).

[37] S. G. Sharapov, V. P. Gusynin, and H. Beck, Phys. Rev. B **69**, 075104 (2004).

[38] K. Kishigi and Y. Hasegawa, Phys. Rev. B **94**, 085405 (2016).

[39] H. Kino and H. Fukuyama, J. Phys. Soc. Jpn. **64**, 1877 (1995).

[40] H. Seo, J. Phys. Soc. Jpn. **69**, 805 (2000).

[41] Y. Takano, K. Hiraki, H. M. Yamamoto, T. Nakamura, and T. Takahashi, J. Phys. Chem. Solids **62**, 393 (2001).

[42] R. Wojciechowski, K. Yamamoto, K. Yakushi, M. Inokuchi, and A. Kawamoto, Phys. Rev. B **67**, 224105 (2003).

[43] N. Tajima, A. Ebina-Tajima, M. Tamura, Y. Nishio, and K. Kajita, J. Phys. Soc. Jpn. **71**, 1832 (2002).

[44] N. Tajima, T. Yamauchi, T. Yamaguchi, M. Suda, Y. Kawasugi, H. M. Yamamoto, R. Kato, Y. Nishio, and K. Kajita, Phys. Rev. B **88**, 075315 (2013).

[45] R. Beyer, A. Dengl, T. Peterseim, S. Wackerow, T. Ivek, A. V. Pronin, D. Schweitzer, and M. Dressel, Phys. Rev. B **93**, 195116 (2016).

[46] D. Liu, K. Ishikawa, R. Takehara, K. Miyagawa, M. Tamura, and K. Kanoda, Phys. Rev. Lett. **116**, 226401 (2016).

[47] T. Mori, A. Kobayashi, Y. Sasaki, H. Kobayashi, G. Saito, and H. Inokuchi, Chem. Lett. **13**, 957 (1984).

[48] T. Mori, J. Phys. Soc. Jpn. **79**, 014703 (2010).

[49] R. Kondo, S. Kagoshima, and J. Harada, Rev. Sci. Instrum. **76**, 093902 (2005).

[50] R. Kondo, S. Kagoshima, N. Tajima, and R. Kato, J. Phys. Soc. Jpn. **78**, 114714 (2009).

[51] H. Kino and T. Miyazaki, J. Phys. Soc. Jpn. **75**, 034704 (2006).

[52] P. Alemany, J. P. Pouget, and E. Canadell, Phys. Rev. B **85**, 195118 (2012).

[53] G. Montambaux, F. Piechon, J. N. Fuchs, and M. O. Goerbig, Eur. Phys. J. B **72**, 509 (2009).

[54] D. J. Thouless, M. Kohmoto, M. P. Nightingale and M. denNijs, Phys. Rev. Lett. **49**, 405 (1982).

[55] M. Kohmoto, Ann. Phys. (NY) **160**, 343 (1985).

[56] M. Kohmoto, Phys. Rev. B **39**, 11943 (1989).

[57] K. Kishigi, M. Nakano, K. Machida, and Y. Hori, J. Phys. Soc. Jpn. **64**, 3043 (1995).

[58] N. Harrison, J. Caulfield, J. Singleton, P. H. P. Reinders, F. Herlach, W. Hayes, M. Kurmoo, and P. Day, J. Phys.: Condens. Matter **8**, 5415 (1996).

[59] M. Nakano, J. Phys. Soc. Jpn. **66**, 19 (1997).

[60] J. Y. Fortin and T. Ziman, Phys. Rev. Lett. **80**, 3117 (1998).

[61] A. S. Alexandrov and A. M. Bratkovsky, Phys. Rev. Lett. **76**, 1308 (1996).

[62] A. S. Alexandrov and A. M. Bratkovsky, Phys. Rev. B **63**, 033105 (2001).

[63] T. Champel, Phys. Rev. B **64**, 054407 (2001).

[64] K. Kishigi and Y. Hasegawa, Phys. Rev. B **65**, 205405 (2002).

[65] B. S. Tan, Y.-T. Hsu, B. Zeng, M. Ciomaga Hatnean, N. Harrison, Z. Zhu, M. Hartstein, M. Kiourlappou, A. Srivastava, M. D. Johannes, T. P. Murphy, J.-H. Park, L. Balicas, G. G. Lonzarich, G. Balakrishnan, and Suchitra E. Sebastian, Science **349**, 287 (2015).

[66] J. Knolle and Nigel R. Cooper, Phys. Rev. Lett. **115**, 146401 (2015).

[67] O. Erten, P. Ghaemi, and P. Coleman, Phys. Rev. Lett. **116**, 046403 (2016).

[68] L. Zhang, X. Y. Song, and F. Wang, Phys. Rev. Lett. **116**, 046404 (2016).

[69] H. K. Pal, F. Piechon, J.-N. Fuchs, M. Goerbig, and G. Montambaux, Phys. Rev. B **94**, 125140 (2016).

[70] G. Li and E. Y. Andrei, Nat. Phys. **3**, 623 (2007).

[71] L. Tarruell, D. Greif, T. Uehlinger, G. Jotzu, T. Esslinger, and J. L. McChesney, Nature (London) **483**, 302 (2012).

[72] Y. Hasegawa and K. Kishigi, J. Phys. Soc. Jpn. **80**, 054707 (2011).

[73] Y. Hasegawa and M. Kohmoto, Phys. Rev. B **88**, 125426 (2013).

[74] A. A. Soluyanov, D. Gresch, Z. Wang, Q. S. Wu, M. Troyer, X. Dai, and B. A. Bernevig, Nature (London) **527**, 495 (2015).